A Study on the Optimization of Dye-Sensitized Solar Cells

by

Md Imran Khan

A thesis submitted in partial fulfillment
of the requirements for the degree of
Master of Science in Electrical Engineering
Department of Electrical Engineering
College of Engineering
University of South Florida

Co-Major Professor: Andrew Hoff, Ph.D.
Co-Major Professor: Christos Ferekides, Ph.D.
Don Morel, Ph.D.

Date of Approval:
March 7, 2013

Keywords: Nanoparticle, Organic Dye, Porosity, Blocking Layer, Electrolyte

ProQuest LLC.
789 East Eisenhower Parkway
P.O. Box 1346
Ann Arbor, MI 48106 - 1346

Dedication

To my respected parents and beloved siblings.

Acknowledgment

This work has become possible with the continuous encouragement and helpful suggestions of lots of wonderful people around me.

I would like to express my heartiest gratitude and sincere appreciation to my co-major professors Dr. Andrew Hoff and Dr. Chris Ferekides for having given me the opportunity to work on this project towards my Master's degree, and also for their guidance and inspiration throughout my research work. Thanks to Dr. Peter Zhang and Dr. Limei Jin, Department of Chemistry, USF for their collaboration in this project. I would also like to thank Dr. Don Morel for agreeing to be in my committee.

I am very grateful to all my fellow researchers and friends; especially Kartikay Singh, Dr. Xianjin Feng, Vamsi Evani, Vishal Kendre and Shamara Collins for their valuable suggestions and help during the research work. I would like to thank my uncle, aunt and cousins, for making my stay in USA like my second home.

This work was supported by the Florida Energy Systems Consortium (FESC) and the College of Engineering, University of South Florida.

Table of Contents

List of Tables

List of Figures

Abstract

Considering biocompatibility, the Dye Sensitized Solar Cell (DSC) based on titanium dioxide should play a major role in the future of solar energy. In this ongoing study, different components and ambient process conditions for the fabrication of were investigated. Titanium dioxide substrate thickness and morphology was found to have a direct impact on the cell efficiency. Scanning Electron Microscopy (SEM) was used to investigate the TiO_2 nanostructure. Different chemical treatments and electrolytes were also explored towards optimizing the cell performance. A group of porphyrin based organic dyes were synthesized and evaluated. Standard solar cell characterization techniques such as current-voltage and spectral response measurements were employed to evaluate the cell performance.

Chapter 1: Solar Energy and Solar Cells

1.1 Introduction

In the modern world of technological advancements, energy has become one of the basic needs for life. With the increase in world population, so is rising the energy demand. The worldwide power consumption is expected to double in the next 3 decades, and the limited supply of fossil fuels is hardly expected to cope with this. Nuclear power, though capable of providing large scale power generation, is being proven to be guilty in safety and waste management issues. Hence, sooner or later we need to turn to renewable energy sources, and the most viable candidate of them is solar energy.

Among all other abundant and non-polluting renewable energy sources (examples include solar, wind, water and geothermal heat) in our planet, solar energy is expected to play a vital role as a future energy source. We receive about 3×10^{24} joule/year energy in the form of sunlight to the earth's surface, which is nearly 10^4 times more than the world's energy consumption.[1] While the sun can provide, we are in need of devising practical approach for conversion, storage and distribution of this energy.

1.2 Solar Cell

Capturing solar energy and converting it to usable forms like electricity or chemical fuels remains a huge challenge. Photovoltaic devices are the primary solar energy conversion systems to harvest the solar energy. These photovoltaic devices, more simply known as

solar cells, convert the incident photon energy of the solar radiation into electrical energy through the generation and subsequent collection of electron-hole pairs. There are several challenges that need to be met for the R&D of solar cell technologies to make it a pragmatic solution to our energy crisis:

- High power conversion efficiency.
- Low cost.
- Long term stability.
- Using abundant and biocompatible raw materials.

1.3 Photovoltaic Generation

Solar cells are categorized into three generations based on their performance and cost effectiveness. The first generation of solar cells has a relatively higher efficiency with expensive production cost. They are the classical example of solar cells. Photo-generated electron-hole pair is separated and collected through the p-n junction of a doped semiconductor, mainly silicon. The commercial market is dominated by this generation.

Thin film solar cells based on CdTe or CuInGaSe make up the 2nd generation cells. They have a lower efficiency, but are much cheaper to produce and employ a less extensive fabrication process. Employing thin film technology the cell thickness has been reduced from millimeter thick down to just a few microns, making possible a production cost of $0.73 per watt in 2011.[2]

The drawback to the 1st and 2nd generations is that they are limited by the Shockley-Queisser theoretical limit of ~30% for a single p-n junction.[3] The 3rd generation solar cells consist of any cells that aren't grouped into the 1st and 2nd generations. They employ a variety of different technologies and are not restrained by the Shockley-Queisser limit.

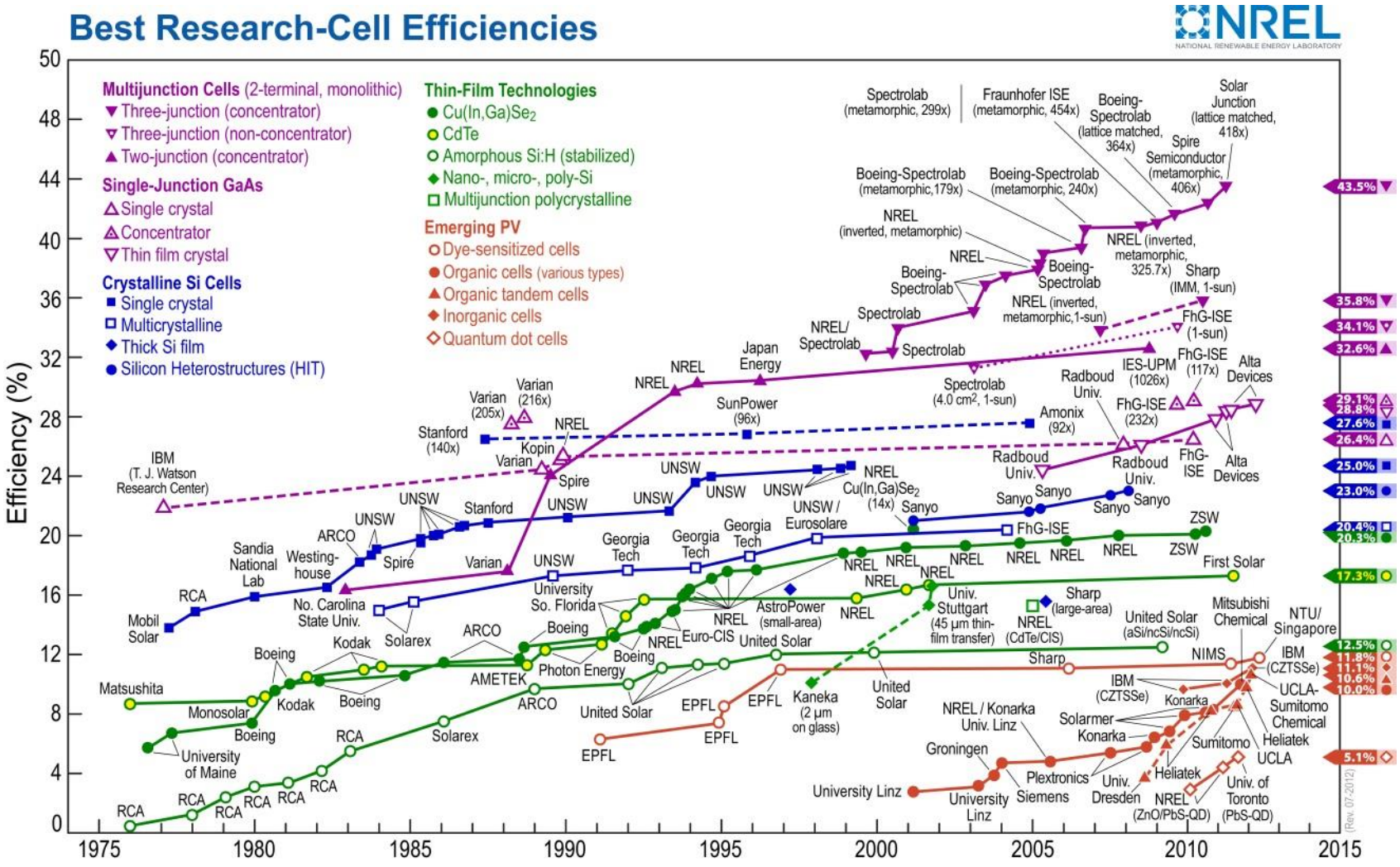

Figure 1.1: Best research-cell efficiency.[4] Reprinted with permission from National Renewable Energy Laboratory. (Refer to Appendix A for details)

Most of the 3rd generation technologies are not yet commercially implemented, but there is a lot of research going on with a promising future. Dye sensitized solar cell is an organic solar cell of the 3rd generation. Figure 1.1 shows the history and current achievements of photovoltaic research in different categories throughout the world.[4]

1.4 Classical P-N Junction Solar Cell

The 1st and 2nd generation photovoltaic devices consist of a p-doped semiconductor and an n-doped semiconductor placed in contact to form a junction. Without the presence of an external applied bias, an electric field is formed at this junction (depletion region) due to the inter-diffusion of majority charges. Photon absorption from sunlight at the depletion region generates electron-hole pair which gets separated by the built-in electric field.

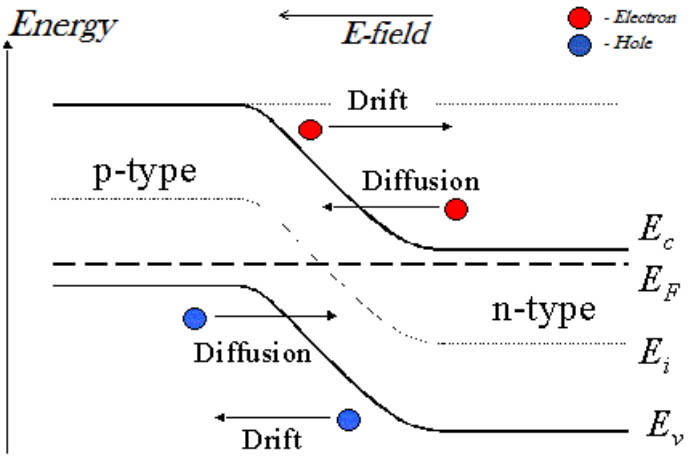

Figure 1.2: Charge separation in a P-N junction.

As long as the separated charges come out of the depletion region, they become the majority carrier and can be collected at the positive and negative contacts giving rise to the cell current.

1.5 Solar Cell Terminologies

A current source in parallel with a forward biased diode expresses the equivalent circuit of an ideal solar cell. Series and parallel resistances are added to account for various loss mechanisms.

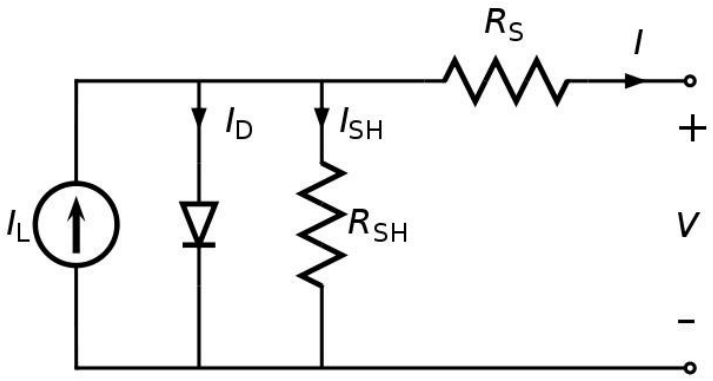

Figure 1.3: Solar cell equivalent circuit.

1.5.1 Short-circuit Current

It is the current obtained from the cell when short circuited or in other words when the load resistance is zero. Solar cell current is normally represented as current density, J_{sc}:

$$J_{SC} = \frac{I_{SC}}{A} \qquad (mA/cm^2) \tag{1.1}$$

where A is the effective area of the solar cell. It is a function of the solar illumination, optical properties and charge transfer probability of the cell.

1.5.2 Open-circuit Voltage

Open-circuit voltage is the maximum voltage available from a solar cell and is obtained when a load with infinite resistance is attached to its terminals. It is a function of the semiconductor bandgap and charge recombination in the cell. For DSC the V_{oc} is given by:

$$V_{OC} = \frac{E_{CB}}{q} + \frac{kT}{q}\ln\left(\frac{n}{N_{CB}}\right) - \frac{E_{redox}}{q} \qquad \text{(volts)} \qquad (1.2)$$

where, n is the number of electron in TiO_2 conduction band and N_{CB} is the effective density of states.[5] The first two terms defines the quasi-fermi level of TiO_2 and E_{redox} is the Nernst potential of the redox mediator.

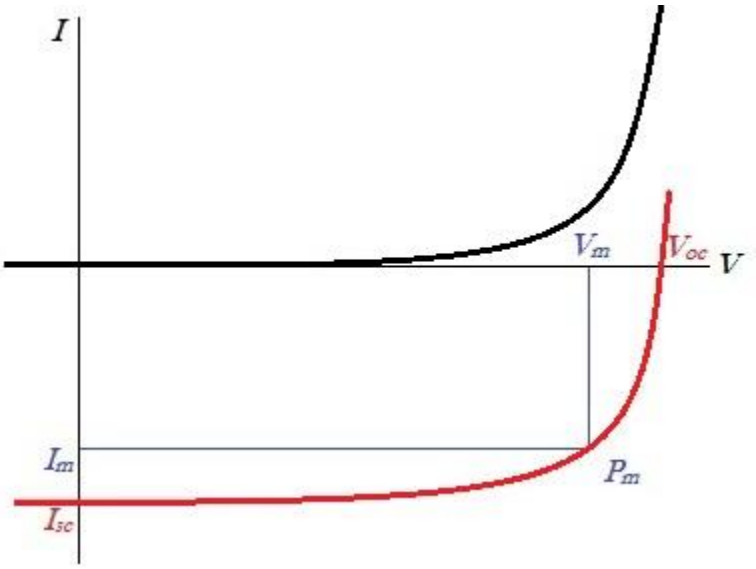

Light I-V response (red line) and dark I-V response (Black line).

Figure 1.4: Typical current-voltage relationship of a solar cell.

1.5.3 Series Resistance

Series resistance, R_S in a solar cell is the result of contact resistance and charge transfer resistance in the semiconductor material. Series resistance reduces the fill factor affecting the maximum power output, while excessively high value of R_S can also reduce the short-circuit current. The open-circuit voltage is not affected since, at V_{OC} the total current flow through cell itself and hence through the series resistance is zero. An approximation of the series resistance can be determined from the slope of the IV curve at the open-circuit voltage point.

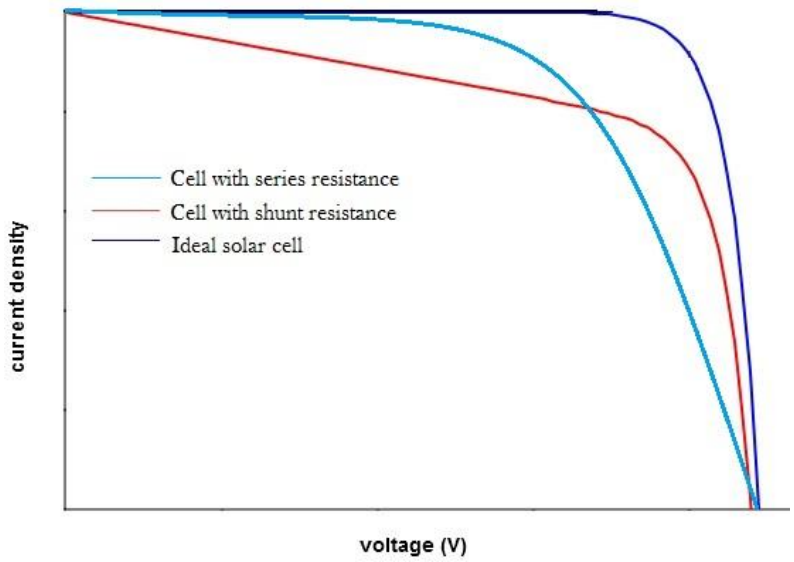

Figure 1.5: Current-voltage response of a solar cell with series and shunt resistance.

1.5.4 Shunt Resistance

Low shunt resistance provides an alternate current path for the photo-generated current causing significant power loss. The effect of low shunt resistance is reduced fill factor and lower open-circuit voltage affecting the maximum power output. The short-circuit voltage is not affected unless for a very low value, since at J_{SC} the total current flows through the outer path and hence through the shunt resistance is low. An approximation of the shunt resistance can be calculated from the slope of the IV curve at the short circuit current point.

1.5.5 Fill Factor

The fill factor (FF) is a measure of the maximum power output from a solar cell. It represents the squareness of the I-V curve and is defined as the ratio of the maximum power to the product of V_{OC} and I_{SC} for the solar cell:

$$FF = \frac{V_m \times I_m}{V_{OC} \times I_{SC}} \tag{1.3}$$

where, V_m and I_m are the voltage and current at maximum power point. Fill factor, being a ratio of the same physical parameters, has no unit. Fill factor is a function of the series and shunt resistance of the solar cell. For DSC, it reflects the extent of electrical and electrochemical losses during cell operation. To obtain higher fill factor improvement of the shunt resistance and decrement of the series resistance, with reduction of the overvoltage for diffusion and charge transfer is required.

1.5.6 Efficiency

The efficiency of a solar cell is defined as the ratio of maximum electrical energy output to the energy input from the sun. Thus the mathematical definition of Efficiency:

$$\eta = \left(\frac{V_{OC} \times I_{SC} \times FF}{P_{in}}\right) \tag{1.4}$$

where, P_{in} is the power input from the sunlight. Efficiency is generally expressed in percentage.

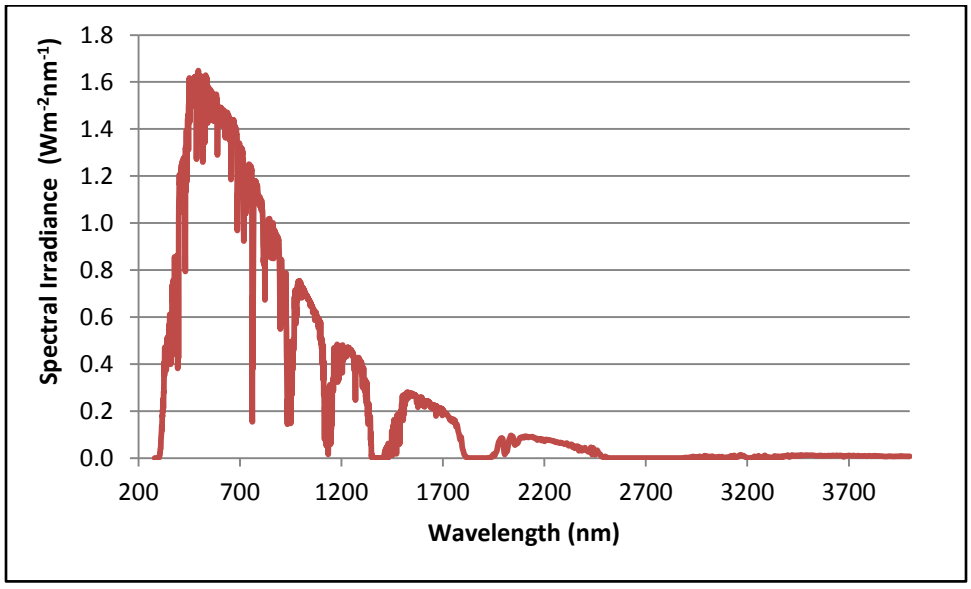

Figure 1.6: 'AM1.5 Global' spectra for solar cell measurement.

Besides the solar cell performance itself, it depends on the incident light spectrum and intensity as well as operating temperature. The internationally recognized standard

condition for the efficiency measurement of solar cells is under 'AM1.5 Global' [6] solar irradiation and at a temperature of 25°C. (Fig. 1.6)

1.5.7 Quantum Efficiency

Quantum efficiency (QE) or 'External Quantum Efficiency (EQE)', sometimes also referred to as Incident Photon to Charge Carrier Efficiency (IPCE) is a measure of how efficient a solar cell is in producing photo-generated charge at a given frequency. It is defined as the ratio of the number of incident photons to the number of charge carriers generated and is a function of the excitation wavelength:

$$\text{IPCE}\ (\lambda) = 1240 \times \frac{I_{SC}}{\lambda \times \phi} \tag{1.5}$$

where, I_{SC} is the short circuit current (mA/cm^2), λ is the wavelength (nm) and Φ is the incident radiative light flux (W/m^2).

For DSC, the term is defined as:

$$\text{IPCE}\ (\lambda) = \text{LHE}(\lambda) \times \phi(\text{inj}) \times \eta(\text{coll}) \tag{1.6}$$

where, LHE(λ) is the light-harvesting efficiency for photons at wavelength λ, Φ(inj) is the electron injection quantum yield for the excited sensitizer to the semiconductor oxide conduction band and η(coll) is the fraction of injected charges that is able to reach the back contact. [7]

Chapter 2: Dye Sensitized Solar Cell

2.1 History

Although the electricity generation capability of organic dyes has been known since late 1960s, the first attempt to generate electricity form dye sensitized semiconductor film was from ZnO sensitized with Chlorophylls[8] and that's why they are sometimes referred as 'Artificial Photosynthesis'. The first embodiment of modern day Dye-sensitized Solar Cell (DSC) dates back to late 1980s.[9] However, not until the fundamental work of Grätzel and O'Regan in 1991,[10] it was proven that DSCs can be a feasible alternative energy source. The highest reported efficiency for DSCs with conventional Ru-based dyes is around 11.5%.[11,12] Recently, a Zn-based dye and Co-based electrolyte pair have been developed and their efficiency has exceeded 12%.[13]

2.2 Advantages of DSC

Although the power conversion efficiency of DSC is not as good as compared to other inorganic 1st and 2nd generation solar cells, it has an edge over them at some points. In the normal operating temperature range of 25–65ºC, DSC efficiency is nearly temperature-independent. For the same range, the efficiency of Si solar cells declines by 20%.[14] In diffuse sunlight or cloudy conditions, DSC shows even better efficiency than polycrystalline Si solar cell. Performance is less sensitive to the incident angle of the light radiation; hence a solar tracking mechanism is less necessary. Although a mass commercial production of DSC is still not available, it can be expected that it has a cost

advantage over all thin film devices. Only low cost and abundantly available materials are needed. Unlike amorphous silicon, CdTe or CIGS cells, DSC can avoid the costly and energy-demanding high vacuum as well as materials purification steps.

DSC materials are biocompatible and abundantly available. The technology can be expanded up to the terawatt scale without facing material supply problems. This gives organic-based solar cells an edge over the 2 major competing thin-film photovoltaic technologies - CdTe and CuIn(As)Se; which use highly toxic materials of small natural abundance. A key requirement for all types of solar cells is long-term stability. From different extensive studies, it has been confirmed that the DSCs can satisfy the stability requirements for commercial solar cells to endure outdoor operation for 20 plus years. Considering these advantages, DSC has the potential to be a feasible candidate for the race of large-scale solar energy conversion systems.

2.3 Basic Operating Principle

The Dye Sensitized Solar Cell (DSC) uses the same basic principle as plant photosynthesis to generate electricity from sunlight. Each plant leaf is a photo-chemical cell that converts solar energy into biological material. Although only 0.02-0.05% of the incident solar energy is converted by the photosynthesis process, the food being produced is 100 times more than what is needed for mankind.[15] The chlorophyll in green leaves generate electrons using the photon energy, which triggers the subsequent reactions to complete the photosynthesis process.

The DSC (a typical configuration is shown in Fig. 2.1) is the only photovoltaic device that utilizes separate mediums for light absorption/carrier generation (dye) and carrier transport (TiO_2 nano-particles). The operation steps are the following.

2.3.1 Excitation

The light is absorbed by a sensitizer dye molecule, it goes over an electronic state change from the ground (S) to the excited state (S*). For most dyes the absorption onset is in the range of 720nm corresponding to a photon energy of 1.72eV. The lifetime of the excited state is in the order of nanoseconds.

$$S + h\vartheta \rightarrow S^* \tag{2.1}$$

$$S^* \rightarrow S^+ + e^- \tag{2.2}$$

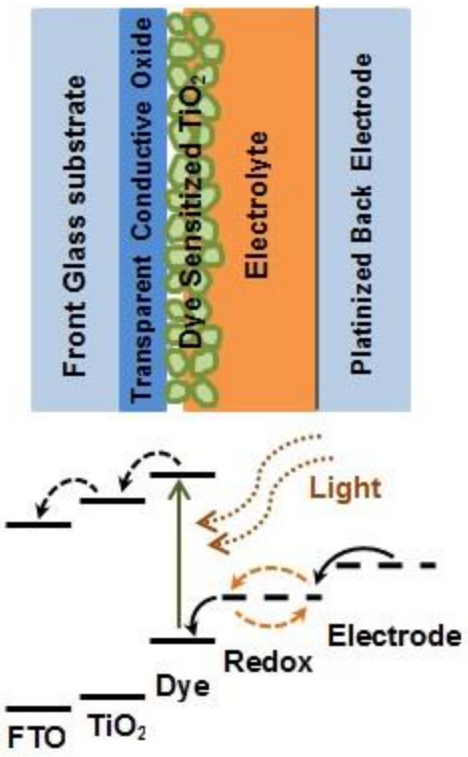

Figure 2.1: Basic device structure and relative band diagram for DSC.

2.3.2 Injection

The sensitizing dye molecules are adsorbed on the surface of a wide band gap semiconductor (typically TiO_2). Upon absorption of a photon (excitation), the dye gains the ability to transfer an electron to the conduction band of the semiconductor. The

internal electric field of the nanoparticles causes the electron extraction and the dye becomes oxidized (S^+). For efficient electron injection the lowest unoccupied molecular orbital (LUMO) of the dye has to be about 0.3 eV above the TiO_2 conduction band. The injection rate constant is in the femtosecond range for singlet state.

2.3.3 Diffusion in TiO_2

The nonporous TiO_2 film consists of spherical anatase particles of diameter ~20 nm. The presence of oxygen vacancies in the lattice makes it a weakly n-doped material (equivalent carrier concentration 10^{16} cm^{-3}).[16] As the TiO_2 particle diameter is too small for electric field to build up, the dominant electron transport mechanism is diffusion via trapping and de-trapping.

2.3.4 Iodine Reduction

The electron travels through the outer circuit performing work, reaches the back FTO electrode, and reduces the iodine in the electrolyte. The platinum layer on the FTO acts as a catalyst for the reduction. The dark cathode reaction:

$$I_3^- + 2e^- \rightarrow 3I^- \qquad (2.3)$$

The iodine reduction can also occur at the excited dye molecules causing recombination of the photo-generated electrons. For efficient charge transfer, the rate of iodine reduction at the counter electrode has to be orders of magnitude faster than the recombination at the TiO_2/electrolyte interface.

2.3.5 Dye Regeneration

The reduced iodide ion replenishes the highest occupied molecular orbital (HOMO) of the dye - regenerating its original form, and makes it ready for electron generation again.

The photoanode reaction:

$$2I^- \rightarrow I_2 + 2e^- \qquad (2.4)$$

This prevents buildup of S^+, which could lead to the conduction band electrons going back to the dye molecules. The maximum output voltage equals to the difference between the Fermi level of the semiconductor and the redox potential of the mediator.[17] Thus, the device is can produce electricity from light without undergoing any permanent physical and chemical change.

2.4 Equivalent Circuit of DSC

The mesoscopic film of the electron transport medium is composed of an array of oxide nanoparticles. In the dark, the DSC behaves as a leaking capacitor. Electron loss in DSC occurs to the electrolyte through the reduction of triiodide ion (I_3^-).

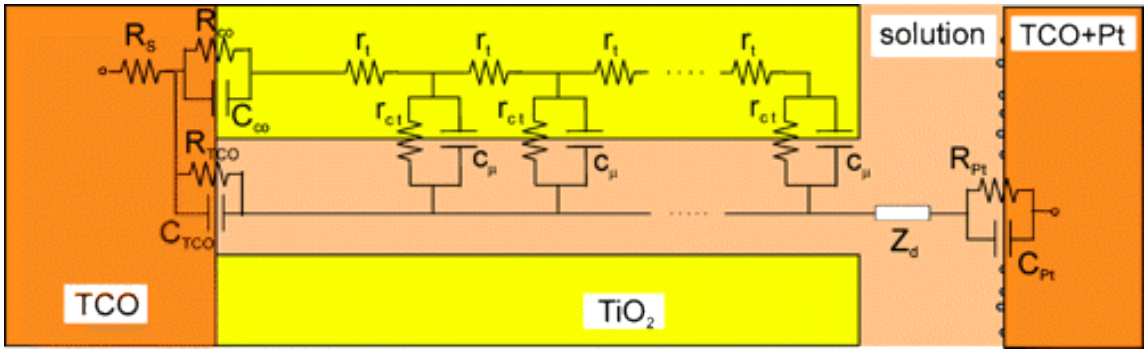

Figure 2.2: Equivalent circuit and general transmission line model of DSC. Reprinted with permission from ACS. (Refer to Appendix A for details)

In the equivalent electrical circuit of DSC (Fig. 2.2) each particle is represented as a resistive element (r_{ct}) coupled to the electrolyte, denoted by the capacitor (C_μ) connected in parallel with the resistance.[18] Among the other terms, r_t is the transport resistance of the electrons in the semiconductor, R_s is the series resistance including the sheet resistance of the TCO glass and the contact resistance of the cell, and Z_d is the

impedance parameter designating the diffusion of I_3^- in the electrolyte. The subscripts Pt, TCO and CO denotes charge transfer resistance and capacitance parameters at the cathode, TCO-electrolyte interface and TCO-TiO_2 interface respectively.

.

Chapter 3: Literature Review

DSC is the only solar cell that separates the two functions of light harvesting and charge-carrier transport. All other conventional and OPV technologies perform both operations simultaneously. This separation opens up a vast amount of options for engineering and optimizing the different parts and functions of the cell individually.

Over the last 2 decades the amount of research in the field of DSC has increased exponentially. In this study, only literatures that are directly relevant to this project are included.

3.1 Semiconductor

Among the many wide-bandgap oxide semiconductors that have been examined as potential electron acceptors for DSC, TiO_2 is the most versatile. It delivers the highest efficiencies, is chemically stable, non-toxic, and available in large quantities. Its anatase nanocrystalline form gives the most efficiency with optimization of surface area, porosity, pore diameter, transparency and film thickness. TiO_2 is the semiconductor of choice due to its wide bandgap, nanoporous structure with large surface area and, suitable HOMO and LUMO alignment with the electrolyte and dye respectively. The rutile phase has a bandgap of 3 eV, while 3.2 eV for anatase; corresponding to photon absorption edge of 413 and 388 nm.[46] In the dark, this wide bandgap semiconductor oxide film is insulating. Due to the nanometer size of the particles (~20nm), a single electron injection produces an electron concentration of 10^{17} cm^{-3} resulting a conductance in the order of 10^{-4} Scm^{-1}

for the electron diffusion coefficient of 10^{-4} cm^2 s^{-1}.[1] Other structures of TiO_2, such as organized meso porous film [19] or TiO_2 nanotubes [20] have also produced comparable efficiency.

Other semiconductor materials have also been employed in DSC. ZnO has identical band gap and band edge positions like TiO_2 with similar crystal structure.[21] Both ZnO nanoparticles [22] and nanotubes [23] have been employed in DSC. ZnO does not require high-temperature annealing process like TiO_2, which enables DSC fabrication on flexible polymer substrates. Other, alternative wide-gap oxides such as SnO_2 [24], In_2O_3 [25], Y_2O_3 [26] and Nb_2O_5 [27] have been under study, and have potential for DSC. Although individual performances of these semiconductors are not so efficient, some of their combinations have shown promising results.

3.1.1 Surface Structure

Two opposing characteristics - film porosity and effective surface area – are the performance defining criteria for DSC. The photo-generated current increases with the increment of surface area, while it decreases with the increase of porosity. Porosity is a measure of the void spaces in a material, and is defined as the fraction of the volume of empty spaces over the total volume, normally represented as a percentage between 0~100. Photo-generated current from the solar cell increases with the increase of surface area due to the availability of more anchoring site for the dyes. An increasing porosity causes to generate less current due to the reduction in the mass of TiO_2 per square centimeter of film as well as the effective TiO_2 surface per square centimeter. Less surface area leads to a lower density of dye molecules adsorbed. Hence, less porosity is desirable.

However, the charge carriers diffuse slowly in the electrolyte in the presence of small pores. In a 4nm diameter pore, the dye molecules absorbed on the pore walls occupy 3nm of it (molecular diameter of dyes ~1.5nm). An aperture of only 1nm is available for the diffusion of the electrolyte, which is close to the size of the tri-iodide ion. Obviously, the transport kinetics is also affected by other parameters, like the electrolyte solvent viscosity and the iodine concentration.[17]

The size, shape, and crystal structure of the TiO_2 nanoparticles depend on the method of preparation of the paste.[28] The porosity is also a function of the annealing temperature profile. The average pore size increases from 15nm to 20nm with an increasing temperature from 400°C. However, with annealing temperatures above 500°C this trend becomes stable with no change in the pore-size distribution.[17] An annealing temperature study from 150°C to 450°C shows an increasing J_{SC} for films annealed at higher temperature, due to higher porosity. This is attributed to the increase of diffusion coefficient and carrier lifetime with increasing temperature.[29]

TiO_2 nanoparticle size is another key parameter for DSC. With increasing particle size electron diffusion coefficient increases due to the decrease of surface area and the structure of grain boundaries. On the other hand, electron recombination lifetime decreases with particle size increase. Thus, a small particle size would be favorable for DSC applications. However, charge injection efficiency is lowered with the decrease of the particle size due to reduced diffusion length. Hence, an optimization in the particle size is the requirement.[30]

The typical film thickness for DSC is 5–20μm with the TiO_2 mass of about 1–4 mg/cm^2. An optimum surface area of the sintered TiO_2 colloid is 75m^2/g and a porosity of 50–65%.[31] For a 10-15 μm thick titania film the effective surface area is increased over a

thousand times, which is the beauty of the mesoscopic structure, allowing for a dense monolayer of adsorbed sensitizer. The nano-particles have an average size of 15-30nm. HRTEM measurements shows that the preferred orientation is (1 0 1) due to its lower surface energy, followed by (1 0 0) and (0 0 1).[32]

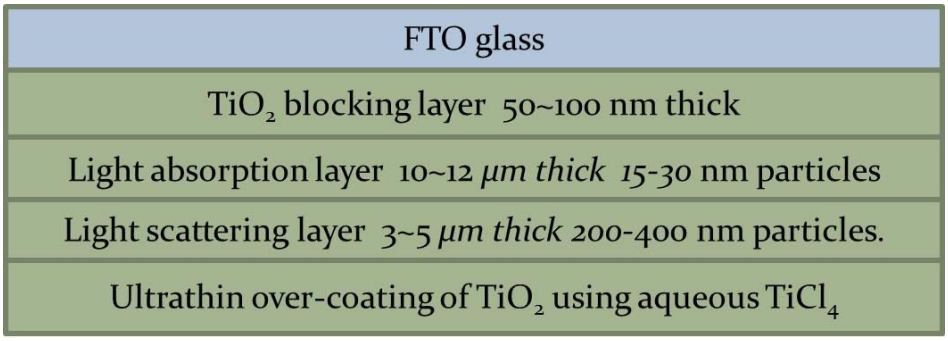

Figure 3.1: TiO_2 structure of DSC for optimum performance.

3.1.2 Semiconductor Thickness

For DSC, the thickness of the TiO_2 layers directly controls the photon adsorption. For single-layer electrodes (20nm particles) a small but linear decrease in the open-circuit voltage (V_{OC}) is observed with increasing thickness. However, thickness response of the short-circuit current density (J_{SC}) depends on the viscosity of the electrolyte. A low viscosity electrolyte can support higher photocurrent generated from thick nanocrystalline-TiO_2 layer, hence the current will exhibit a linear rise. However, for high viscosity electrolyte a peak in the current is observed and after that, it decreases. The thickness dependence is also a function of particle size and surface structure. For example, optimal thickness for 20nm particles is half of that obtained for the 42nm particles. [33]

3.1.3 Light Scattering Layer

One limitation of the sensitizing dyes is their poor performance in the near infra-red spectrum of light. A way of improving this is - by introducing an additional light scattering layer of larger titania particles. These can be mixed with or screen-printed on top of the film of 15-30nm sized TiO_2 particles. This allows the scattered photons to be contained in the film by means of multiple reflections, increasing their optical path length substantially beyond the film thickness. Consequently, the solar light absorption is enhanced, especially in the red to near-IR regions. With the use of 200-400nm sized anatase particles as light-scattering centers, an increment of the J_{SC} by 3-4 mA/cm^2 was observed for N719-based DSCs because of the enhanced light absorption.

Moreover, approximately 4% loss occurs because of the reflection of incident light on the glass substrate. This can be partially overcome by introducing an anti-reflecting film, which can also act as a UV cut-off filter.[37]

3.1.4 Blocking Layer

Charge recombination is one of the main reasons of lower current for DSC. Recombination occurs at both Electrode/Electrolyte and TiO_2/Electrolyte interface. A compact blocking layer of TiO_2 by RF sputtering[34] or spray pyrolysis[35] between the conducting electrode and the nanocrystalline TiO_2 layer can effectively prevent the recombination at electrode/electrolyte interface. Introduction of this layer prevents electrolyte from reaching the electrode (increases J_{SC}) and also enhance electron transport from nanocrystalline titania to the electrode (increases V_{OC}). This blocking layer is absolutely necessary for planar organic dyes, while ruthenium based sensitizers can perform this anode insulation themselves against recombination losses.[36]

A rather cost effective and easier way of incorporating this blocking layer is through hydrolysis of $TiCl_4$. $TiCl_4$ treatment on FTO substrate is found to suppress the dark current, shifting its commencement by some hundred millivolts. This is due to a positive shift in the conduction band edge of highly doped SnO_2 by about 0.5 V which results in a higher electron density in the FTO substrate.[37] This blocking layer can also be made of other metal-oxides such as ZnO or Nb_5O_2. [38]

3.1.5 $TiCl_4$ Treatment

To reduce charge recombination at TiO_2/electrolyte interface, another blocking layer of TiO_2 is implemented via $TiCl_4$ treatment with subsequent annealing. The average pore diameter and specific surface area decreases with the $TiCl_4$ treatment, because of the surface epitaxial growth of TiO_2, resulting in particle-necking and a new TiO_2 layer. The increase of the inter-particle necking will reduce the resistance in electron transport through the nanoparticles reducing the recombination probability. At the same time, it improves the surface roughness factor and light absorbance.[37] These lead to a decrease in the dark current and an increase of the photocurrent.[39] Hydrolysis from the acidic $TiCl_4$ solution prevents deposition of impurities in the $TiCl_4$, such as Fe^{3+}, because of the higher solubility of iron oxide compared to TiO_2. The P25 powder, which is the most common source of producing nanocrystalline Titania, contains as far as 100 ppm of Fe_2O_3, which is known for causing interference with electron injection from the excited state of the dye. The $TiCl_4$ treatment covers this relatively impure semiconductor core with a TiO_2 thin layer of ultra-high purity. This improves the injection efficiency and the blocking character of the semiconductor-electrolyte junction.[46]

Theoretically, this overlayer can be formed of other metal–oxide films (examples include MgO, ZnO, Al_2O_3, and Nb_2O_5) which have conduction band edges higher than TiO_2. [40]

The performance of these oxides depends on their protonation / deprotonation capability of the TiO_2 surface, which enhances dye adsorption and a positive shift of the TiO_2 flat band.[41] For example, Al_2O_3 being basic, will tend to deprotonate the TiO_2 film, resulting in the improvement in cell performance.

3.2 Dye

The photo sensitizer dye is the heart of operation of DSC. Upon sensitization of the semiconductor film, the dyes form a monomolecular coating, with the stoichiometry of the anchored photosensitizer as high as ~1:100 (Ru per Ti).[42] Stringent engineering of the dye is necessary for efficient light absorption, charge injection and collection of the cell.

3.2.1 Design Considerations for Efficient Photosensitizer

- Spectral response: The light absorption properties of the dye must be tuned to have maximum visible light response.
- Charge transfer: For efficient charge transfer, the excited state of the dye needs to be aligned to the acceptor orbitals of the semiconductor. An electronic coupling of the LUMO of the dye to the titanium 3d orbitals is required.
- Functional group: The functional groups on the dye control the adsorption on the semiconductor surface and facilitate electron transport between excited state of the dye and the TiO_2 conduction band.[43]
- Redox potential: The reduced state of the dye should be tuned to the reduction potential of the redox mediator to have efficient hole transfer reactions in the electrolyte medium. A preferable potential difference of about 0.3 eV is required to ensure that dye regeneration rate is fast

enough to minimize the electron recombination between the semiconductor conduction band and the oxidized sensitizer.[32] While a larger difference is beneficial to reduce this recombination further, but that results in the loss of output potential.

- Stability: To compete with existing technologies, it should have a guaranteed lifetime of about 20 years corresponding to about 10^8 redox reaction cycles.

3.2.2 Areas of Improvement

Although the absorption spectra of most efficient sensitizers today are between 400–800nm, their efficiencies are quite low in the near infrared to infrared region. For the commercially available dye that achieved the highest efficiencies so far (Black Dye), the HOMO level is at -5.0 eV [44] which is only marginally lower than the HOMO (-4.9 eV) of the redox couple. On the other hand, the LUMO is at about -3.5 eV, which is significantly higher than the TiO_2 conduction band (4.0 eV). Reduction of the band gap of the dye would allow it to absorb light in the near infra-red region.

Downshifting of the sensitizer LUMO level is an opportunity to synthesize more efficient dye, but will reduce the electron injection efficiency and increase the charge recombination. Hence, a way of improving the short circuit current and hence the efficiency of DSC is to increase the electron injection efficiency and reduce the charge recombination.[45]

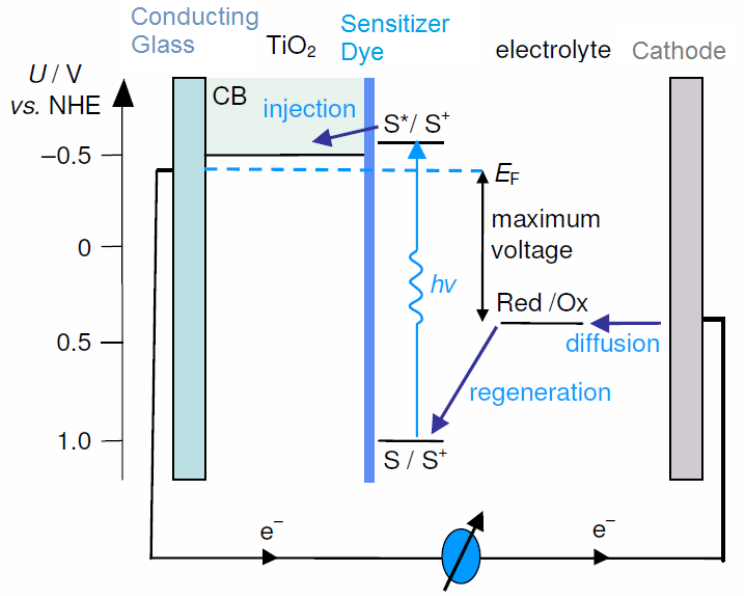

Figure 3.2: Energy band diagram of DSC. Reprinted with permission from WSPC. (Refer to Appendix A for details)

3.2.3 Black Dye

The most successful commercially available sensitizers employed so far in DSC are different polypyridyl-type ruthenium complexes producing power conversion efficiencies of up to 11% with stable performance for millions of turnovers. Invention of Black Dye in 1992 for the first time achieved more than 10% efficiency for DSC.[46] Its broad range of light absorption (visible to near IR) and having comparatively long lifetime excited state make it an attractive sensitizer for DSC. Its photocurrent onset is around 900 nm which corresponds to a band gap of 1.4 eV. This is close to the optimum threshold absorption wavelength for single-junction photovoltaic cells.

The carboxylate groups linked to the bipyridyl moieties ensure intimate adsorption to the oxide semiconductor surface such as TiO_2, providing strong electronic coupling and necessary wave function manifold to the conduction band of the semiconductor for efficient ultrafast electron injection with near 100% quantum yield.

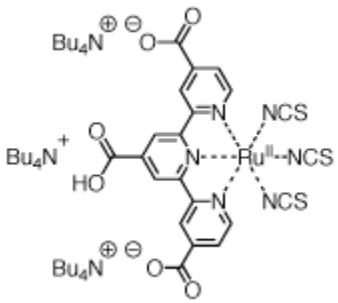

Figure 3.3: Chemical structure of N-749 (black dye). Reprinted with permission from Solaronix SA. (Refer to Appendix A for details)

3.2.4 Anchoring Group

The photo-sensitizer is attached onto the semiconductor surface through anchoring groups. It ensures that the dye molecules are spontaneously assembled on the semiconductor surface upon the exposure to a dye solution. Different anchoring groups such as - carboxylate, phosphonate or hydroxamate – bind the dye molecules to the semiconductor oxide by coordination of titanium ions.

The anchoring group is responsible for efficient charge injection and dye orientation on the titania surface. In most cases dyes with carboxylate anchoring groups outperform those with more strongly attached phosphonate groups. ATR-FTIR measurements show that carboxylate group binds itself onto the titanium oxide surface by bidentate chelation.[56]

3.2.5 Degree of Protonation

The anchoring groups of the sensitizer contain protons. Light adsorption causes most of its protons to be transferred to the semiconductor surface, making it positively charged. This causes the Fermi level to move down positively. This increases the adsorption of the dye molecules and enhances electron injection from the excited sensitizer state into the semiconductor conduction band due to the electric field from the surface dipole,

generating higher photocurrent. Nonetheless, this Fermi level shift results in lower open circuit voltage because of the decrease in the gap with the redox couple.

On the other hand, the presence of zero protons in the sensitizer moves the Fermi level negatively (upward) due to the adsorption of anions and cations. This results in an increased open-circuit potential but with low short circuit current. Therefore, an optimal degree of sensitizer protonation is required. [47] [48] [49]

3.2.6 Dye Additives

The presence of dye additive like Cheno is essential for avoiding surface aggregation of the sensitizer molecules.[50] Macrocyclic organic dyes like porphyrins have an issue with solution aggregation rather than attaching to the titania surface due to π-stacking on to the TiO_2. One possible way to prevent this - a bulky molecule such as chenodeoxycholic acid is added with the solution during the dye-sensitization process.[51]

3.2.7 Dye Structure

A change in the molecular design of the dye can significantly influence the recombination dynamics .The two primary factors controllable by molecular design for adjustment of the interfacial electron-transfer kinetics are the spatial separation from the HOMO orbital of the dye cation to the electrode surface and the energy difference between the electrode Fermi level E_F and the dye oxidation midpoint potential. However, modulation of dye oxidation potential, determined from solution-phase electrochemistry, is limited by the required energy difference for dye cation regeneration reactions (electron injection from redox mediator). Hence, the crucial factor influencing the reaction rate is spatial separation; an increase in which by 3 Å resulted in more than 10 fold increase in the recombination half-time.[52]

One possible way of avoiding dark current in DSC due to charge recombination is to cover the surface, after the adsorption of dye, with hydrophobic chains.[53] Several amphiphilic Ru dyes perform this successfully by having both hydrophilic and lipophilic groups. The presence of the hydrophobic groups on the sensitizer also increases the stability of DSC by water desorption.[54]

3.2.8 Dye Combinations

An option to obtain an extended light absorption throughout the visible and near infra-red spectrum is to use a combination of dyes which have complementary spectral features. Such dye combinations with optimized choice of the agents (mixtures of different porphyrins and phthalocyanines), showed enhanced photovoltaic effects compared to single dye sensitization.[32]

An alternative approach of co-sensitization is by introducing two spatially separated layers of different sensitizer dyes. A secondary metal oxide layer (Al_2O_3) is deposited for the absorption of the second sensitizer, energetically aligned to achieve effective hole transfer from the inner dye.[55]

3.2.9 Porphyrins

Again taking into consideration of the term ‘biocompatibility’, the most efficient dyes to date are based on ruthenium and there is scope for being skeptic about their biocompatibility. Moreover, ruthenium has a very limited supply in nature; making it unsuitable for mass production of DSC. Ruthenium based dyes have been under extensive research for the last 2 decade and it is safe to assume that their maximum efficiency has already been reached.

Porphyrin is a group of organic compounds having intense light absorption in the visible spectra. Given their crucial role in photosynthesis (Chlorophyll is an example of porphyrin), their vast diversity and controllable electrochemical properties make them a potential candidate for DSC.

The absorption spectra of different anchored porphyrin on TiO_2 show responses similar to their corresponding solution spectra. However, emission spectra of the porphyrin adsorbed films are inhibited due to lower the electron injection efficiency from the excited singlet state into the TiO_2 conduction band.[56] Cell efficiency was also found to be dependent upon porphyrin metalation, type and position of acid binder anchoring group, binding solvents as well as the electrolyte.

3.2.10 Design Considerations for Porphyrin Synthesis

- Push-pull porphyrin: Introduction of strong electron donating groups at phenyl rings attached to the porphyrin core can increase the electronic density of the porphyrin π-system. The acid binding group works as the pull factor, improving the electron injection greatly.[57]
- Long chains: Incorporation of long-chain alkyloxy groups in the dye structure can wrap the porphyrin core preventing dye aggregation. It also forms a blocking layer on the TiO_2 surface retarding the unwanted charge recombination reactions.[13]
- Metal base: The Zn derivatives of porphyrin exhibited superior efficiencies over other corresponding metal derivatives.[58]
- Binding group: In terms of DSC performance, the position (meta, para) of the functional groups has a greater influence than the type of those. For Zn-metalloporphyrin, para substitution of the binding group is the best performing, then decreasing towards meta and ortho.[59]

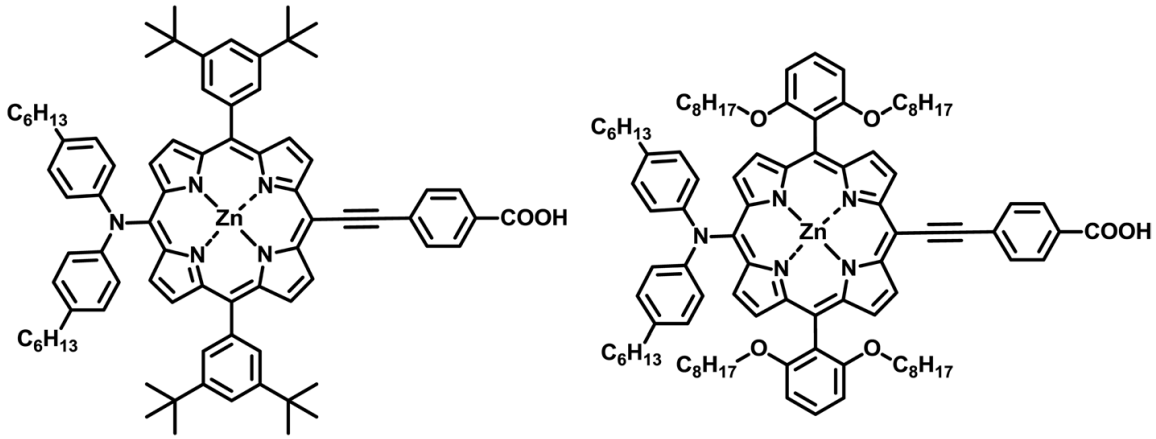

Figure 3.4: Chemical structure of Zn based porphyrin dye, producing best reported efficiency of 12.3% so far for DSC. YD2 (left) and YD2-o-C8 (right). Reprinted with permission from AAAS. (Refer to Appendix A for details)

3.3 Electrolyte

The voltage produced in DSC is determined by the difference between the chemical potential (Fermi level) that the electrons acquire in the TiO_2 nanoparticles and the hole chemical potential in the hole conducting medium (for redox electrolytes, the Nernst potential). In the dark at equilibrium the Fermi level is constant throughout the device. From Equation 1.2, it is evident that V_{OC} can be improved by down-shifting the HOMO level of the redox couple.

Another reason for the need of new electrolyte material is the stability concerns. Liquid electrolyte in the conventional DSCs today is the main cause for the low long term stability. Organic solid redox couples seem to be a viable solution in this regard.

3.3.1 Electrolyte Components

Incorporation of 4-tertbutylpyridine in the electrolyte increases the open-circuit voltage and fill factor by decreasing the dark current at the semiconductor-electrolyte junction. The following relation holds for regenerative photo-electrochemical systems,

$$V_{OC} = \left(\frac{kT}{e}\right) \ln\left(\frac{I_{inj}}{n_{cb} K_{et} [I_3^-]}\right) \quad (3.1)$$

where I_{inj} is the charge flux from sensitizer injection, K_{et} is the rate constant for triiodide reduction and n_{cb} is the electron concentration on the semiconductor surface.[46] Although the TiO_2 surface is covered by a dye monolayer, the reduction of triiodide by conduction band electrons causes the dark current. Due to its relatively small size the triiodide ions either cross the monolayer or have entrance to nanometer-sized pores into which the dye molecules cannot enter. In the latter case, the surface of TiO_2 is exposed to redox mediator. 4-tert-butylpyridine effectively decreases the rate of the reduction of triiodide, increasing the open-circuit voltage of the cell (Eq. 3.1).

When incorporated into DSC electrolyte, ionic liquids can act as both the source of iodide and the solvent itself. Different imidazolium iodide based molten salts improves the stability features of DSC. Although they limit the iodide ion transport speed due to higher viscosity than the solvent, they facilitate long term operation of DSC.[32]

Proton transfer from the anchoring groups of the dye establishes a surface electric field on the TiO_2 surface which produces a charged dipole monolayer. Li^+ or Mg^{2+} ions may be used to charge the surface positively. Li^+ can penetrate deeply into the mesoporous TiO_2 structure due to small radius.[60] This potential gradient from the sensitizer (negative potential) to the oxide (positive potential) can enhance the electron transfer to the semiconductor. Moreover it also prohibits the electrons from returning to the dye after injection, reducing charge recombination.[1] Thus incorporation of LiI in the electrolyte can increase electron transport speed and enhance J_{SC}.

Current DSC implementations mostly use the iodide/triiodide electrolyte system, which due to an excessive potential loss during the dye-regeneration reaction, limits the

maximum obtainable V_{OC} to 0.7~0.8V. Recently, introduction of cobalt based electrolytes, has improved the V_{OC} as high as 0.95V.[13]

3.4 Counter Electrode

Platinum coated FTO glass substrate is used to as the counter electrode for DSC. A light reflecting RF sputtered 2-pm-thick Pt mirror can reflect back the light that passes through the film to maximize light absorption, while also serves as a catalyst for the cathodic reduction of triiodide ion.[46] However, for a nanoporous titania film fully optimized for efficient light absorption, chemically deposited platinum from a solution of 0.05 M hexachloroplatinic acid can perform alike.

3.5 Substrate

The electrode substrate TCO affects the cell performance in 2 ways. The sheet resistance of the FTO influences the series resistance of the cell and the transmittance control the light absorption. Considering sheet resistance, the lower the better, but lower FTO sheet resistance require thicker FTO layer causing reduced light transmittance and efficiency. Optimum value of sheet resistance for TCO is found to be 10Ω/□ with a corresponding light transmittance of 80%.[61]

3.6 Light Intensity and Temperature

The short circuit current shows a linear increase with light intensity due to the presence of more photons and hence more photogenerated electrons. The open-circuit voltage also increases slightly with light intensity. But a decrement in fill factor is observed due to ohmic losses in the conducting glass electrodes.[46]

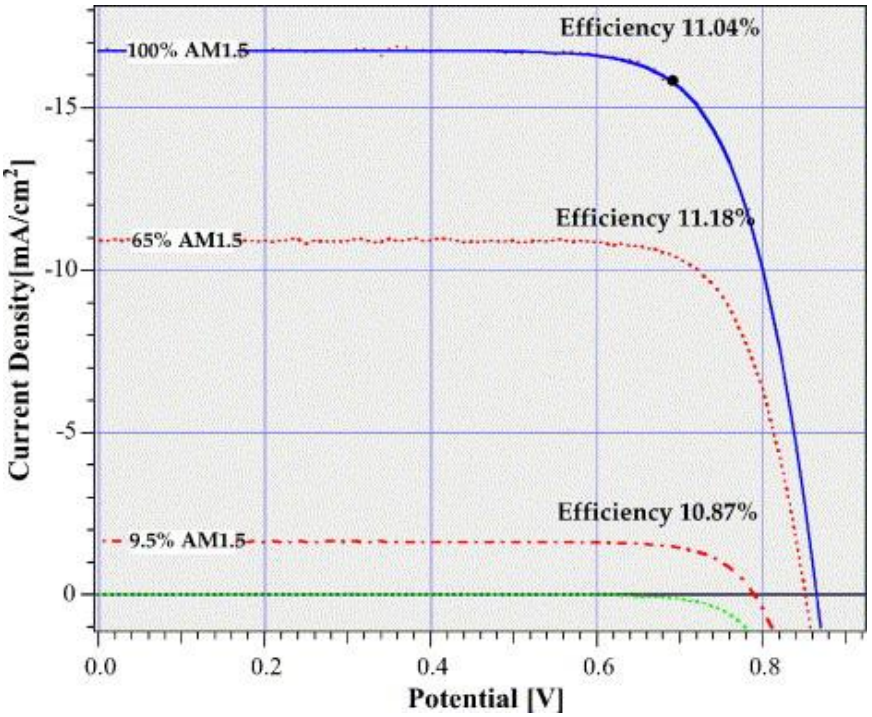

Figure 3.5: Stable performance at diffuse sunlight is a big plus point for DSC. Reprinted with permission from Elsevier. (Refer to Appendix A for details)

Increasing the temperature decreases V_{OC}, while the current rises significantly (5 to 70ºC). The influence on the fill factor is dependent upon the electrolyte solvent. For solvents with high viscosity such as propylene carbonate, the fill factor increases with temperature. The voltage decrease is because of the increment of the dark current with temperature, which implies an increase in the rate constant of triiodide reduction. The quantum efficiency values are not affected within the temperature range. An important observation is that the sensitized charge injection rate is independent of temperature, which implies a quantum mechanical tunneling process. The effect of temperature on the cell efficiency is minor due to the different compensating factors, which is another advantageous feature for DSC. [46]

Chapter 4: Experimental Details

4.1 Materials and Chemicals

- Tin Oxide coated glass electrodes, 3 mm thick, 14 Ω/□, Pilkington
- Anatase TiO_2 nanoparticle colloid, Ti-Nanoxide D/SP, Solaronix
  Particle size 15-20nm with >100nm diffusing particles.
- Black Dye N749, Ruthenizer 620-1H3TBA, Solaronix
- Electrolyte: Iodolyte Z-150, Solaronix
- Acetonitrile anhydrous 99.8%, Sigma-Aldrich
- tert-Butanol - anhydrous ≥99.5%, Sigma-Aldrich
- Deoxycholic acid ≥99%, Sigma-Aldrich
- Titanium (IV) chloride - puriss. ≥99.0%, Sigma-Aldrich
- Platinum precursor solution: Platisol T, Solaronix
- Platinum precursor paste: Platisol T/SP, Solaronix
- Lithium iodide, 99.9% trace metals basis, Sigma Aldrich
- 1,2-Dimethyl-3-propylimidazolium Iodide, TCI America
- 4-tert-butylpyridine, 96%, Sigma Aldrich
- Iodine, crystalline, 99.99+% metals basis, Alfa Aesar
- Polyethylene glycol 20000, Alfa Aesar
- Ethylene glycol anhydrous, 99.8%, Sigma Aldrich
- Sealant: Meltonix 1170-60PF, Solaronix

4.2 Preparation of Working Electrode

The TiO_2 electrode, where the sunlight is absorbed, is called the working electrode.

4.2.1 Cleaning

Tin Oxide (TO) glass was cut into 2cm square pieces. Each of the pieces was cleaned with the following procedure:

- Sonicate in soap solution – 15 min.
- Rinse with copious deionized (DI) water.
- Sonicate in 0.1M HCl – 5 min
- Sonication in Acetone – 5 min
- Sonication in Isopropanol - 5 min
- Boil in Isopropanol (80°C hotplate) – 5 min

4.2.2 Apply Titania

A 1×1 cm^2 window was cut in a piece of Scotch Magic tape (~50-60 um thick) and put on the conductive side FTO glass. A thin film of nano-crystalline TiO_2 was applied onto the conducting glass by 'doctor blading' with a Pt coated blade. The paste was stirred manually before use, but shaking the bottle itself would cause air bubble formation preventing good deposition. The tape was removed carefully and the paste was allowed to relax for 30 min in a covered pertidish. The latter was a critical step as it allows reducing surface irregularity and brings the air bubbles out. Plastic and glass labware were used as much as possible in every steps of the fabrication, as iron contamination is found to have a detrimental effect on cell performance. The thickness of the films was controlled using different blading guides and pressure. Table 4.1 shows different blading guide and achieved titania thickness after annealing. The thickness was measured with an alpha step profilometer.

Table 4.1: Different thickness guide and obtained post-sintering TiO_2 thickness.

Thickness Guide	Average Thickness (um)
Stainless steel foil 12.5um	1.5
Stainless steel foil 25um	3
Scotch Magic Tape 810 1x with pressure	5
Scotch Magic Tape 810 1x	8
Scotch Magic Tape 810 2x with pressure	9
Scotch Magic Tape 810 2x	11
Scotch Magic Tape 810 3x	16

4.2.3 Sintering

The TiO_2 coated substrates were put on a graphite plate inside a glass tube, heated with halogen lamp with reflector setup under dry air flow. The temperature was precisely controlled with a Eurotherm 2208e temperature controller. Different annealing temperature rise rate and final temperatures were experimented, while the following at Table. 4.2 was used as the benchmark temperature profile.

Table 4.2: Standard annealing profile for TiO_2 paste.

Temperature (^{0}C)	Time (min)	Temperature Rise Rate (^{0}C/min)
100	10	30
325	5	30
375	5	10
450	15	15

4.2.4 Preparation of $TiCl_4$ Solution

$TiCl_4$ reacts with water in an exothermic reaction, heating up the solution while making. Moreover, at higher temperature (even at room temperature) it oxidizes into TiO_2.

First, a 2M concentrated stock solution was made. Ice cold deionized (DI) water is taken. $TiCl_4$ vapor is extremely dangerous for inhalation. In an inert gas environment $TiCl_4$ was added slowly to water in an ice bath while being stirred with a magnetic stirrer. A clear transparent solution indicates a good workable solution. The solution was stored in a

freezer. Second, the stock solution was diluted by adding it to cold DI water. Fresh diluted solution was made before each $TiCl_4$ treatment.

4.2.5 $TiCl_4$ Treatment

As the titania electrode has cooled down, polyimide Kapton tape with silicone adhesive was put by the open edges of the electrode to protect the SnO_2 coating on glass. The substrate was kept immersed in $TiCl_4$ solution at 70°C for 30 min in a closed container. The electrode was rinsed with DI water and ethanol. It was then placed back to the heater, dried for 15 min at 80°C and annealed at 500°C for 10min with 5°C/min rise rate. When cooled to 100°C, the electrode was immersed in dye solution.

4.3 Dye Solution

The dye solution (3×10^{-4}M) was prepared in acetonitrile and tert-butyl alcohol as solvents in equal proportion. Deoxycholic acid was added as a co-adsorbent (20mM). The solution was stirred for 30 min and stored in sealed container for 24 hours before use. The dye solution is always needed to be stored away from light. The electrodes were immersed in the dye solutions and then kept overnight at room temperature to adsorb the dye onto the TiO_2 surface. They are kept in the dye until being used in a cell.

4.4 Preparation of Counter Electrode

Two 0.8mm diameter holes were made on a piece of 2×2 cm^2 TCO glass. The cleaned substrate is heated for 15 min at 450°C to remove the residual organic contaminants. A thin layer Pt was deposited on the TO glass by brush painting (for the Platisol T solution) or by doctor blading (for the Platisol T/SP paste). The solution is light sensitive. The electrode was heated immediately at 450°C for 15 min, activating the platinum layer for working. The activated electrodes were instantly used for cell making.

4.5 Cell Fabrication

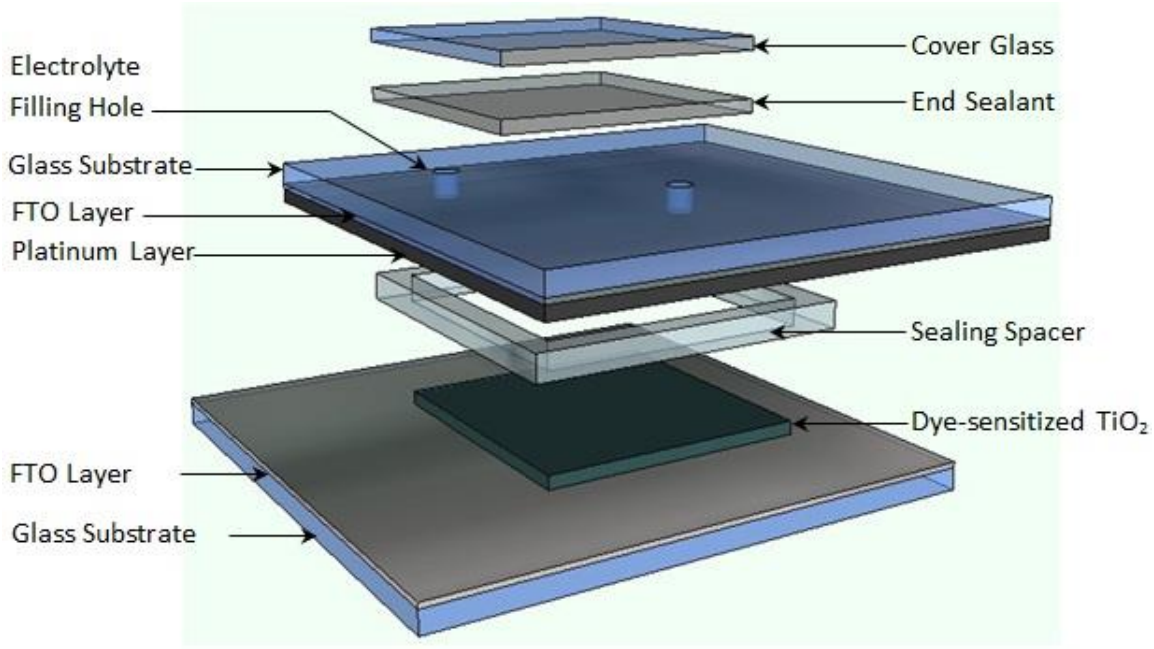

Figure 4.1: Simplified cell structure for DSC

Upon dye sensitization, the TiO_2 electrode was assembled into a sandwich like structure with the Pt-counter electrode. A square gasket was cut out of the sealant spacer material. The inner dimensions should match with the titania film, and the outer dimensions 3mm bigger on all four sides.

The working electrode was taken out of dye solution, carefully rinsed with ethanol and dried with N_2 flow. The sealant gasket was placed around and the counter electrode was put on it while the Pt film faces the titania. Heating at 120°C would seal the electrodes. The electrolyte solution was inserted through one of the holes making sure there is no air bubble inside.

The glass surface was cleaned with acetone wetted wipes and the holes were sealed with another piece of sealant and a cover glass. The space left for contact was painted with silver paint to make better contact. The solar cell should be ready to work!

Chapter 5: Results and Discussions

5.1 Semiconductor Thickness

Optimum thickness was found to be critical to the performance of DSC. With the increase of thickness, there were more dye molecules present in the titania layer to absorb the sunlight, hence an increase in current generation was observed. However, with the increase of thickness it required a longer path for the photo-generated electrons to reach the working electrode thus increasing electron recombination. So, current started decreasing after an optimum thickness.

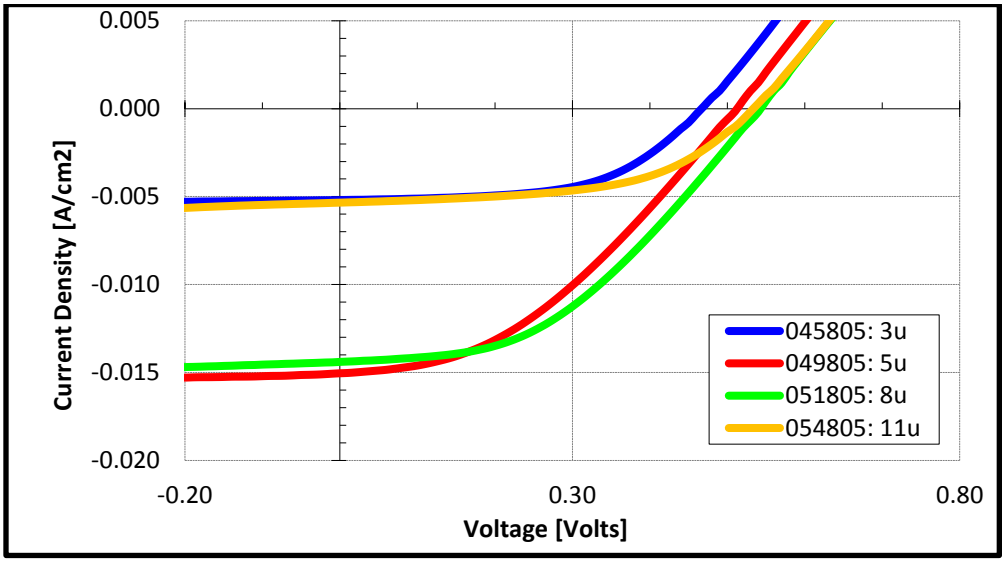

Figure 5.1: Current – voltage relationship for DSC with varying TiO_2 layer thickness. {Black Dye 0.3mM – Iodolyte - (Annealing 325/375/450^{0}C - 30/10/15^{0}C/min) – (Standard $TiCl_4$ treatment, Anneal 500^{0}C - 35^{0}C/min) – Platisol T}

Table 5.1: DSC with varying TiO_2 layer thickness.

Thickness (um)	ID	V_{oc} (V)	FF	J_{sc} (mA/cm^2)	Efficiency (%)
3	045805	0.47	0.557	5.2	1.36
5	049805	0.51	0.394	15.05	3.02
8	051805	0.54	0.435	14.4	3.38
11	054805	0.53	0.548	5.34	1.54

Literatures suggested a slight decrease in open-circuit voltage with the increase in thickness, but the change in observed voltage for the investigated thicknesses was within the range of experimental error.

5.2 Porphyrin Dye

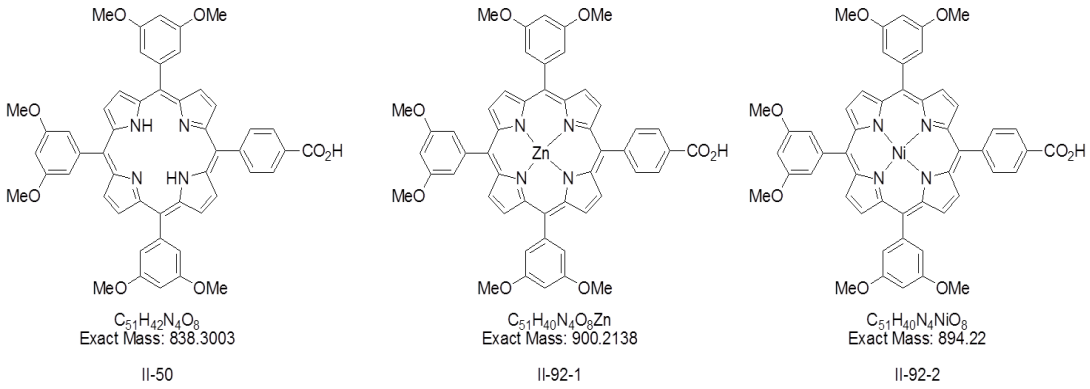

Figure 5.2: Chemical structure of synthesized porphyrin dyes.

As an early part of the project, a group of push-pull (D-π-A) porphyrins were synthesized and used to make DSCs. Methoxy group was used as electron donor and carboxylic acid group as anchor. A free base without any metal (II-50), a zinc-based (II-92-1) and a nickel-based (II-92-2) porphyrins were fabricated as a start. Two different concentrations of the dye solution were investigated, and also a combination of the synthesized dyes, denoted (I+II+III).

Table 5.2: DSCs with synthesized porphyrin dyes.

Dye	Dye Conc. (mM)	Voc (V)	FF	Jsc (mA/cm2)	Efficiency (%)
II-50	0.2	0.37	0.607	0.714	0.16
	0.4	0.4	0.561	1.07	0.24
II-92-1	0.2	0.39	0.625	1.12	0.27
	0.4	0.4	0.613	1.4	0.34
II-92-2	0.2	0.36	0.632	0.218	0.05
	0.4	0.36	0.624	0.23	0.05
I+II+III	0.2	0.39	0.629	0.72	0.18
	0.4	0.31	0.613	0.797	0.19
Black Dye	0.3	0.54	0.435	14.4	3.38

Only somewhat promising dye among the tested ones was Zn-based II-92-1, although not comparable to the black dye. A little dependence on dye concentration was observed, with a slight increase in performance. Nevertheless, from other experiments, this difference became more subtle as the sensitization time was increased. The homogeneous mixture of these 3 dyes was tested and not surprisingly, the resulting cell performance resembled the mathematical average of the three individual cells.

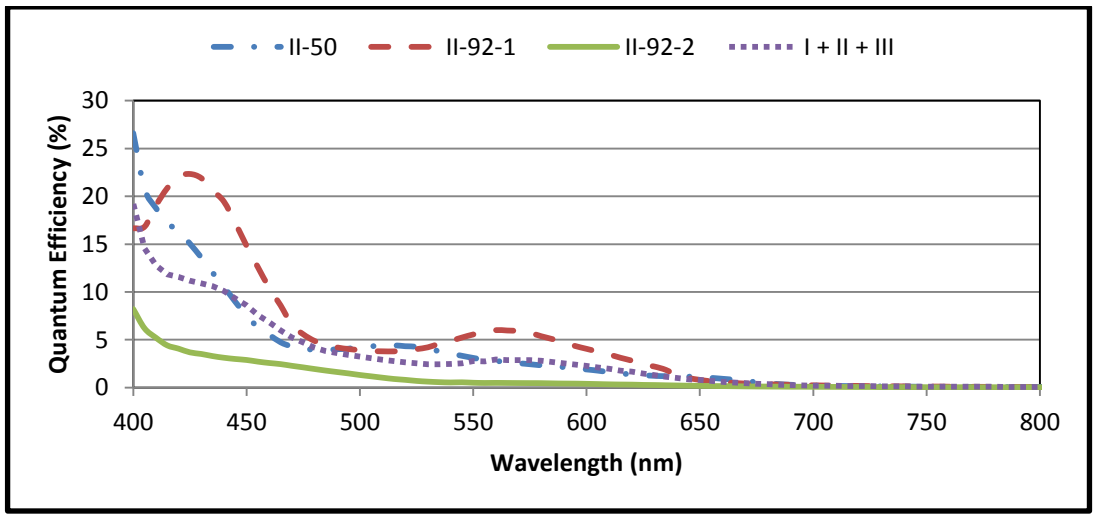

Figure 5.3: Quantum efficiency of DSCs made with porphyrin dyes.

UV-Vis spectra of the dyes (Fig. 5.4) showed a very high absorbance in UV to low frequency of the visible range for the porphyrin dyes, but lacked in near infra-red region. From similar analysis for Black dye (Fig. 5.5), its absorbance was observed not to be very intense but expanded over the whole visible region more evenly.

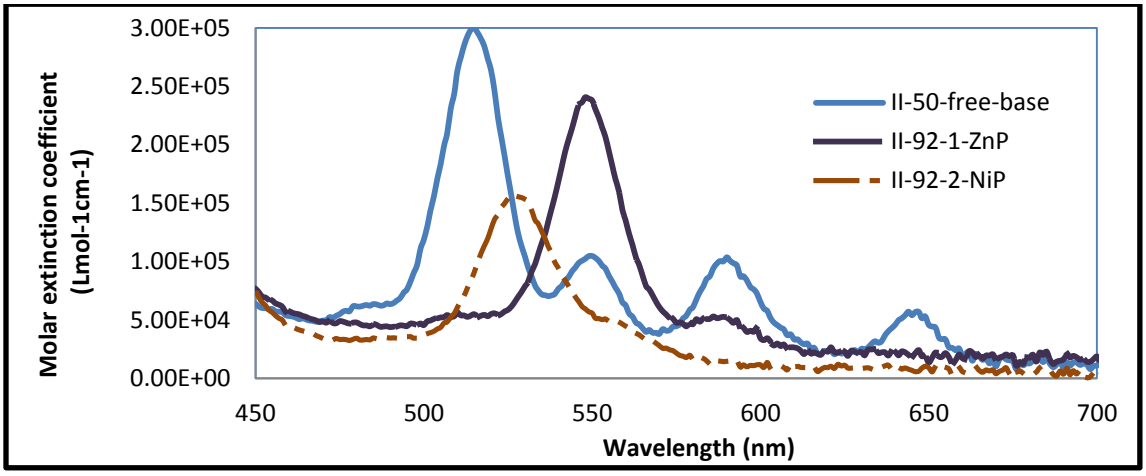

Figure 5.4: UV-Vis spectra of synthesized porphyrin dyes.

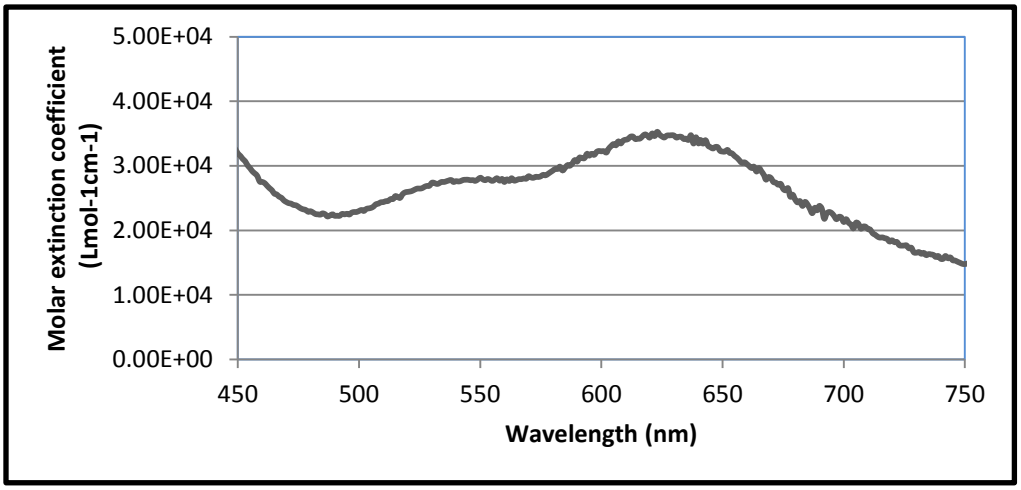

Figure 5.5: UV-Vis spectra of commercial black dye. (4.98 x 10^{-5} M in DCM).

Hence it could be concluded that light absorbance was not a problem with these dyes. It should be the band alignment and charge transfer properties, which was the reason for low efficiency for these porphyrin dyes.

The best reported dye in terms of solar cell efficiency so far is a Zn-based porphyrin dye (Fig 3.3). Design criteria for efficient porphyrin dye are mentioned in section 3.2.10.

5.3 $TiCl_4$ Treatment

An ultra-high purity TiO_2 layer were deposited on the nanocrystalline titania by Chemical Bath Deposition in 50mM aqueous $TiCl_4$ solution for 30 min at 70^0C, followed by a 450^0C thermal annealing. The solution concentration was varied to optimize the effect.

Table 5.3: Effect of $TiCl_4$ treatment for DSC

$TiCl_4$ Concentration (mM)	Voc (V)	FF	Jsc (mA/cm^2)	η (%)	Series Resistance (Ω/cm^2)
0	0.52	0.558	4.3	1.25	35.9
20	0.53	0.546	6.5	1.88	27.8
50	0.47	0.552	8.9	2.3	15.3

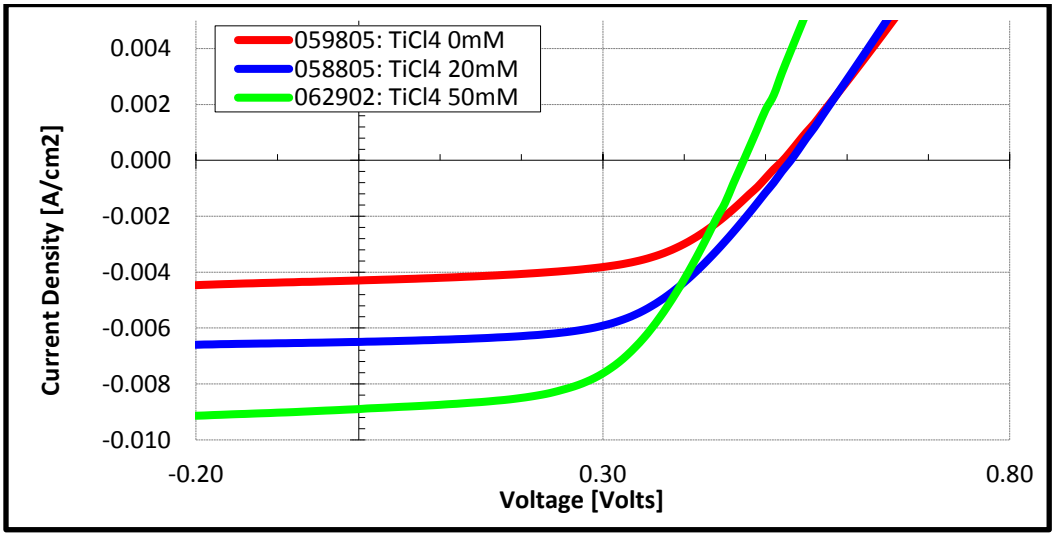

Figure 5.6: Current – voltage relationship for DSC with different concentrations of $TiCl_4$ treatment. {Titania thickness 8um, (Annealing $325/375/450^0$C – $30/15/10^0$C/min), ($TiCl_4$ treatment anneal 500^0C - 30^0C/min), Black Dye, Iodolyte, Platisol T}

Any concentration higher than 50mM of $TiCl_4$ for the treatment made the film to flake. As the $TiCl_4$ solution being slightly acidic in nature,[62] at sufficient concentration it acted as an etchant for TiO_2 nanoparticles and could cause flaking. Incorporation of $TiCl_4$ treatment increased the cell current. During thermal treatment the absorbed $TiCl_4$ inside the titania nanoparticles get oxidized and increased surface porosity causing improved dye loading. Due to enhanced inter-particle necking and reduced charge recombination (section 3.1.4), a decrease in series resistance and increase in short-circuit current were observed with the incorporation of $TiCl_4$ treatment and with increase of its concentration.

5.4 Blocking Layer

5.4.1 RF Sputtered Blocking Layer

A blocking layer of RF sputtered TiO_2 was deposited on clean FTO glass. The sputtering was done with a Titanium target, in presence of O_2 (3.4mTorr) and Ar (6mTorr) at room temperature. Incorporation of an RF sputtered blocking layer decreased both the current and the voltage. With an increase in blocking layer thickness, more decrease is observed.

Table 5.4: DSCs with different thickness of RF sputtered TiO_2 blocking layer.

Blocking Layer Thickness (nm)	Cell ID	**Voc (V)**	**FF**	**Jsc (mA/cm^2)**	**η (%)**
0 nm	751110	0.67	0.486	12.96	4.22
20 nm	920120	0.63	0.536	10.77	3.63
50 nm	950120	0.63	0.532	10.39	3.54
100 nm	980120	0.61	0.521	9.96	3.17

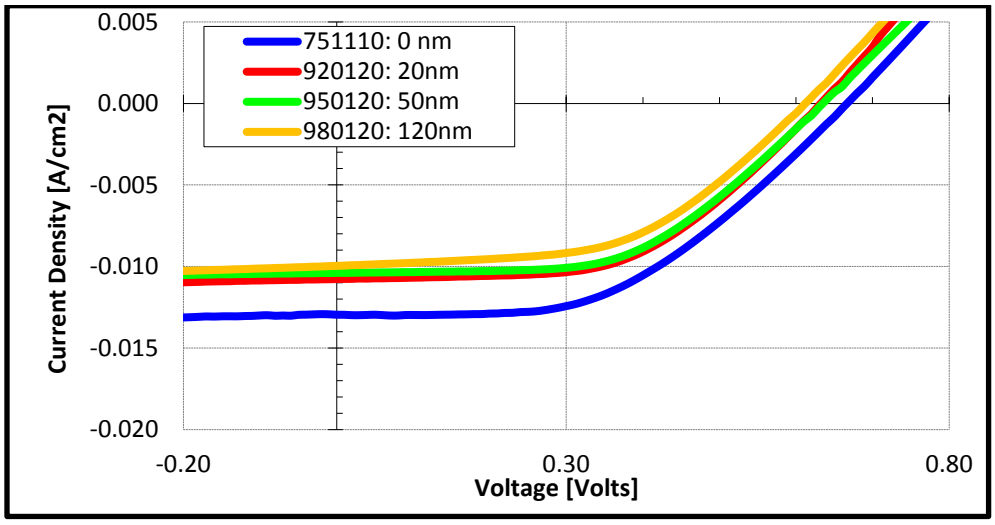

Figure 5.7: Current –voltage relationship for DSC with varying blocking layer thickness. {Titania thickness 8um, (Annealing 325/375/450/500^{0}C - 5^{0}C/min), (Standard TiCl4 treatment, Anneal 500^{0}C - 30^{0}C/min), Black Dye, Electrolyte I, Platisol T}

5.4.2 Chemical Bath Deposition (CBD) Blocking Layer

An thin TiO_2 blocking layer were deposited on the TCO substrate by Chemical Bath Deposition in 50mM aqueous $TiCl_4$ solution for 30 min at 70^{0}C.

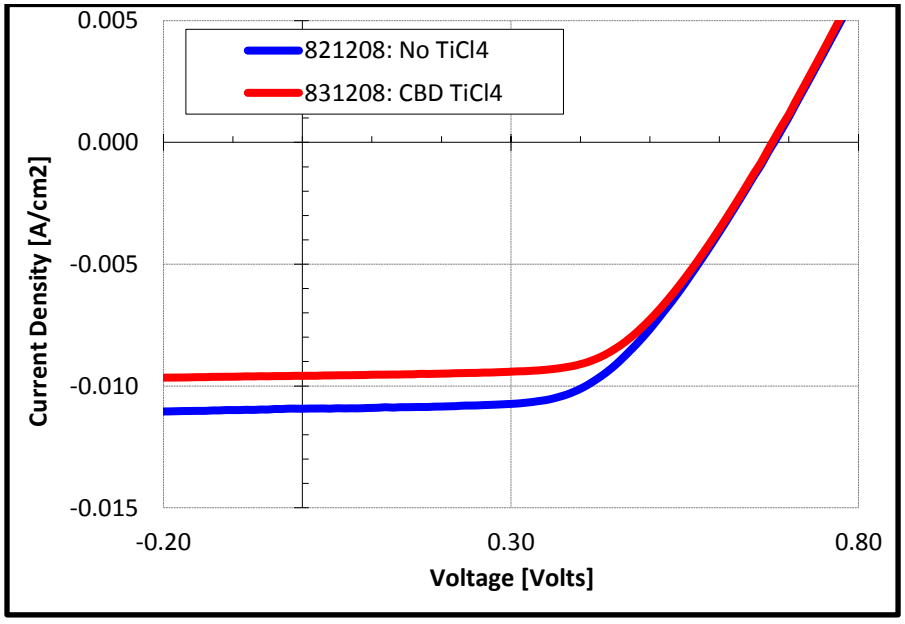

Figure 5.8: Current –voltage relationship for DSC with and without CBD blocking layer. {Titania thickness 11um, (Annealing 325/375/450/500^{0}C - 5^{0}C/min), (Standard $TiCl_4$ treatment, Anneal 500^{0}C - 30^{0}C/min), Black Dye, Electrolyte I, Platisol T}

Table 5.5: Comparison between DSC with and without CBD TiO_2 blocking layer.

CBD Blocking Layer	V_{oc} (V)	FF	J_{sc} (mA/cm^2)	η (%)
No $TiCl_4$	0.68	0.555	10.94	4.13
$TiCl_4$	0.68	0.585	9.59	3.81

Chemical Bath Deposition deposited the thinnest possible blocking layer, which also decreased the current. The purpose of the blocking layer was to prevent charge recombination at the semiconductor/electrode interface, by preventing the electrolyte ions from reaching the electrode. However, for a titania film not optimized for porosity, the nanoporous film itself could effectively block the electrolyte. In that case, introduction of a blocking layer could just cause added series resistance reducing cell performance, which was probably the situation in these experiments.

5.5 Porosity and Surface Area

TiO_2 film porosity is the single most important parameter for DSC. In this study, thermal and chemical manipulation of film porosity was investigated.

5.5.1 Thermal Processing

Annealing temperature profile plays an important role in the film porosity. Annealing of titania in a stepped manner was found to have considerable effect on the nanoparticle structure, and hence on cell performance. Stepped annealing produced highly porous and smaller grain film; while un-stepped annealing produced compact and larger grain size. From Scanning Electron Microscope (SEM) image of the annealed film, it was obvious that stepped annealing produced smaller grains and highly porous surface (Fig. 5.9 a, b). Lower V_{oc} (due to more charge recombination as the electrolyte can go into the semiconductor film) and higher J_{sc} (due to more dye absorption on the titania surface)

with lower series resistance was observed for stepwise annealed cells (Table 5.6, Fig. 5.10).

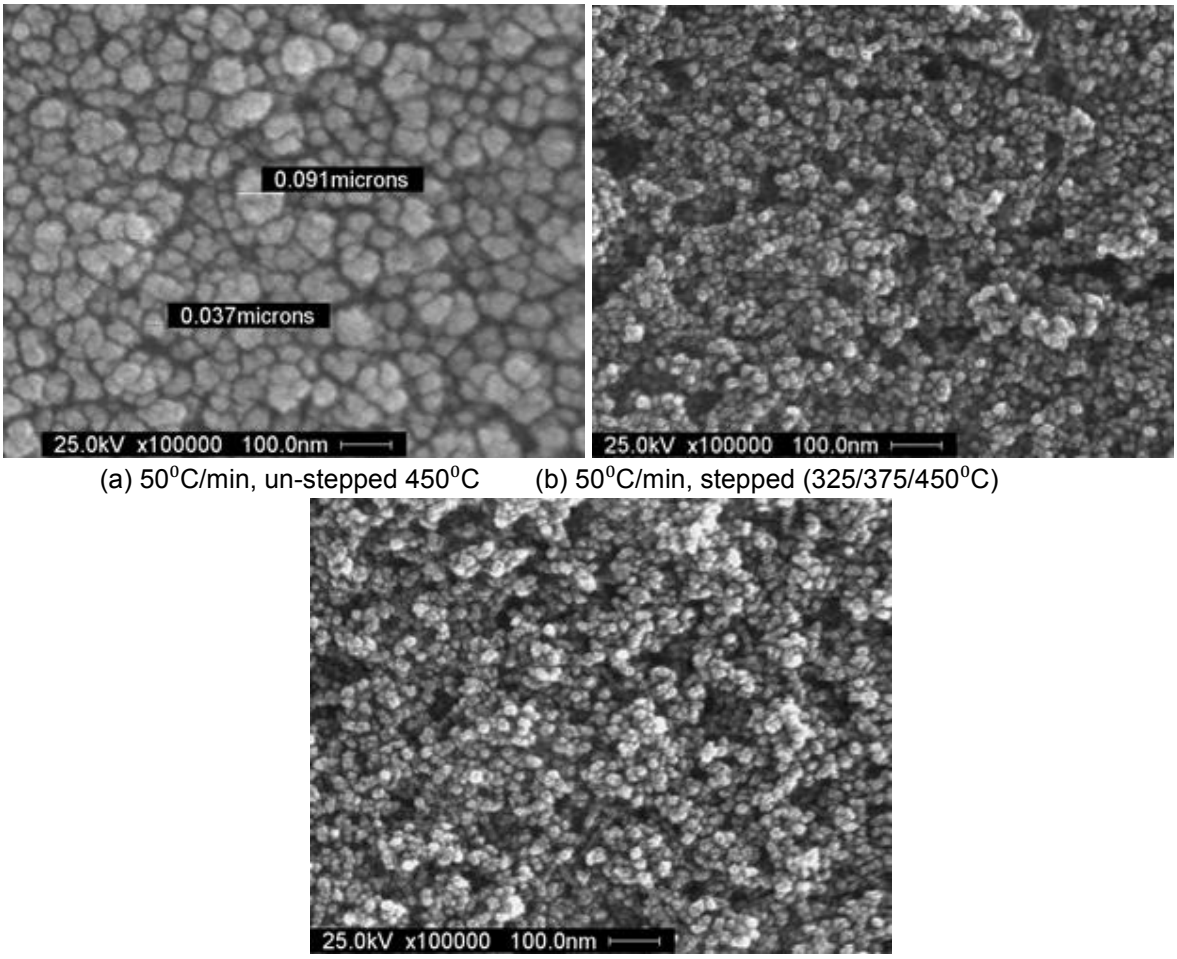

(a) 50^{0}C/min, un-stepped 450^{0}C (b) 50^{0}C/min, stepped (325/375/450^{0}C)

(c) 5^{0}C/min, stepped (325/375/450^{0}C)

Figure 5.9: SEM images for titania electrode annealed at different temperature profile.

Table 5.6: DSCs performance variation for stepped and un-stepped annealing.

Annealing Process	V_{oc} (V)	FF	J_{sc} (mA/cm2)	η (%)	R_s (mΩ/cm^2)
Un-stepped 400^{0}C	0.56	0.45	8.17	2.09	21.5
Stepped 325/375/450^{0}C	0.51	0.394	15.05	3.02	17.6

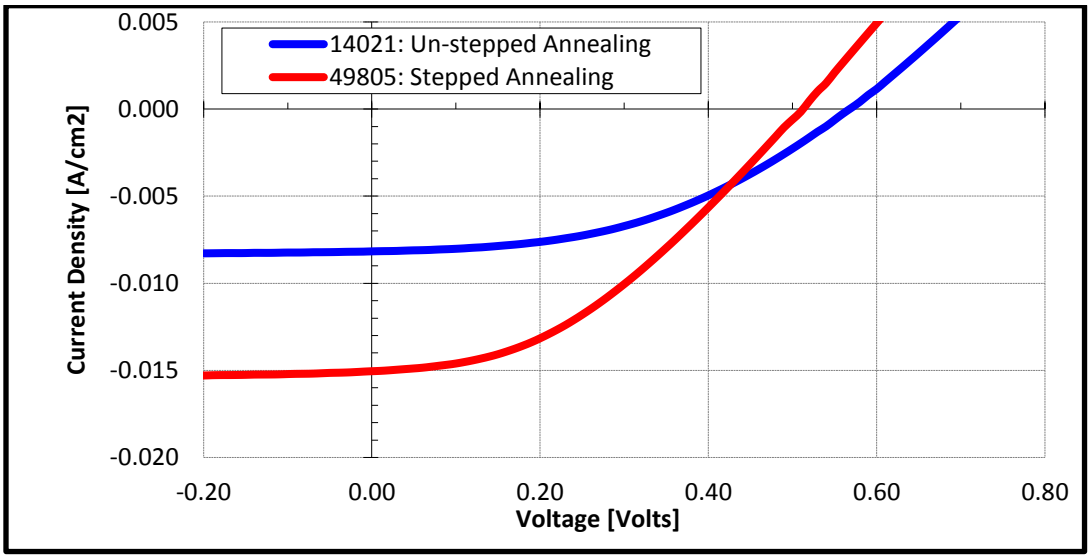

Figure 5.10: Current –voltage relationship for DSC with and without stepwise annealing. {Titania thickness 5um, Standard $TiCl_4$ treatment, Black Dye, Iodolyte, Platisol T}

Annealing temperature rise rate was found to have a boosting effect on cell performance, although no discernible impact on titania structure could be observed from SEM images (Fig. 5.9 b, c). However, current – voltage data of the cells (Table 5.7, Fig. 5.11) showed lower V_{OC} and higher J_{SC} with lower R_S for cells annealed at faster rate. The same trend was observed in the stepped annealing experiment for higher porosity titania nanostructure. Thus, it was conclusive that higher annealing temperature rise rate produced higher porosity film. However, slow rise rate allowed making higher thickness TiO_2 film without flaking, essential for high performance cells. For this reason, slower annealing rate was used for subsequent experiments.

Table 5.7: DSCs performance variation with annealing temperature rise rate.

Annealing Rate	V_{oc} (V)	FF	J_{sc} (mA/cm2)	η (%)	R_s (mΩ/cm^2)
50 C/min	0.64	0.521	12.14	4.05	17.3
5 C/min	0.67	0.518	10.63	3.69	18.5

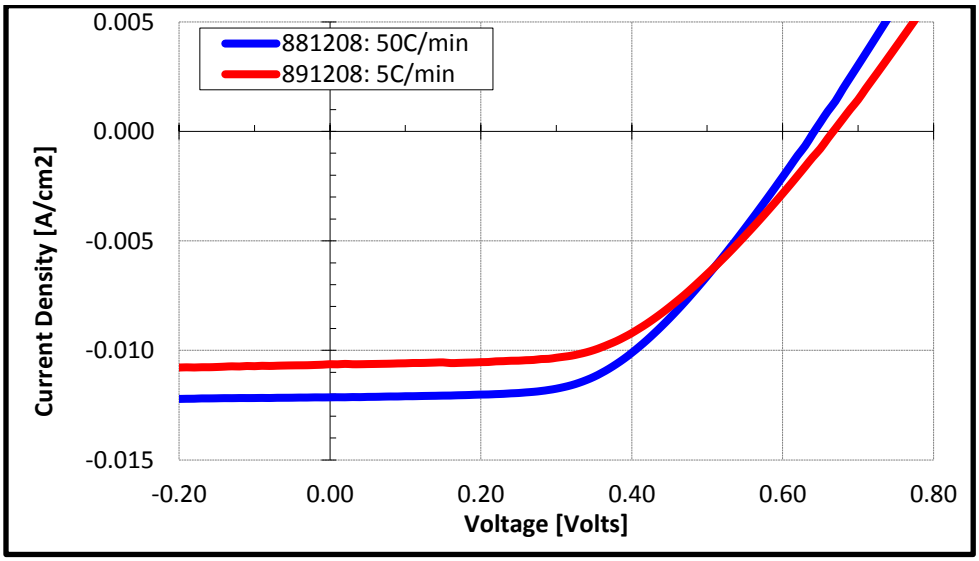

Figure 5.11: Current –voltage relationship for DSC annealed at different temperature rise rate. {Titania thickness 8um, Annealing 500ºC, (Standard $TiCl_4$ treatment, Anneal 500ºC), Black Dye, Electrolyte I, Platisol SP}

5.5.2 Chemical Processing

Titanium dioxide nonporous film structure is highly dependent on the preparation process, components and ambients. Film porosity is a function of Ethylene Glycol (EG) or Polyethylene Glycol (PEG) content of the titania paste.

The vendor 'Solaronix' couldn't disclose the paste content for business policy. EG and PEG were mixed with the paste at different concentrations to alter film porosity. Adding PEG at any concentration cracked the film; possibly being a powder, it didn't mix properly with the paste and put significant stress on the film while evaporating out during sintering.

However, adding 12 wt% EG with the commercial Titania paste (0.1ml EG in 0.86g paste) produced a highly porous film, possibly too porous as it reduced the current. SEM image showed a high porosity film with large holes which is detrimental to cell performance.

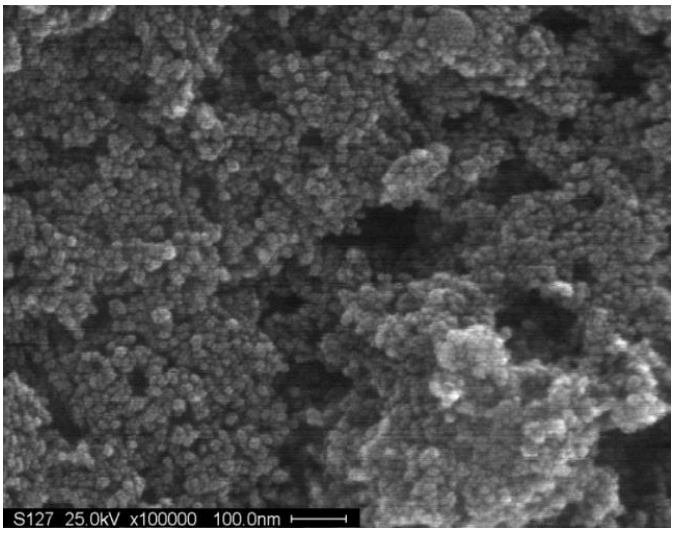

Figure 5.12: SEM image of annealed titania film with 12 wt% EG

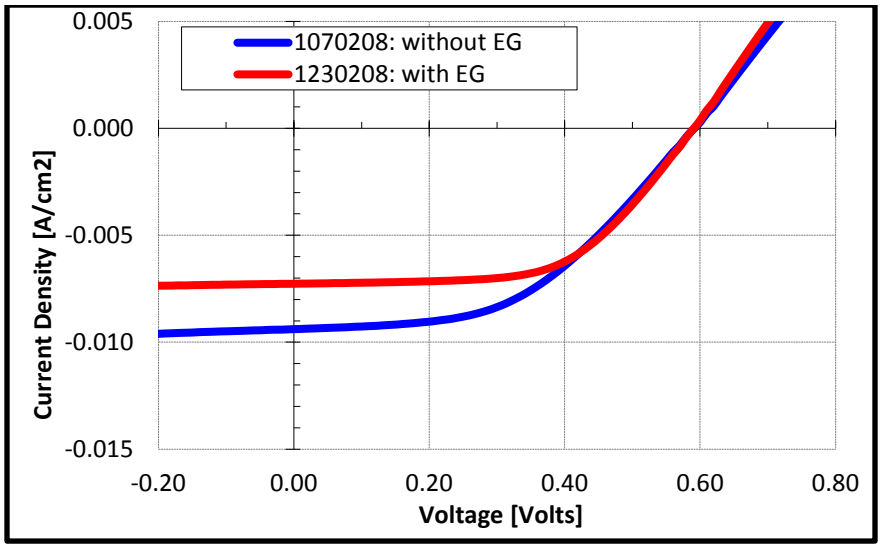

Figure 5.13: Current –voltage relationship for DSC with added EG to titania. {Titania thickness 8um, (Annealing 325/375/450/500ºC - 5ºC/min), (Standard $TiCl_4$ treatment, Anneal 500ºC - 5ºC/min), Black Dye, Electrolyte I, Platisol SP}

Table 5.8: DSC performance with added ethylene glycol to alter surface porosity

Titania	V_{oc} (V)	FF	J_{sc} (mA/cm2)	η (%)	Series Resistance (Ω/cm^2)
Commercial	0.59	0.479	9.39	2.65	39.4
With 12 wt% EG	0.59	0.581	7.27	2.49	31.9

5.6 Electrolyte

Two different electrolytes were studied and their performance in DSC was observed.

- Commercial Electrolyte - Iodolyte Z150
- Electrolyte I - LiI 0.1M, I_2 - 0.05M, DMPII - 0.6M and Tert-Butyl Pyridine - 0.5M in Acetonitrile solvent.

DSC performance with Iodolyte was analyzed in Section 5.1. Similar experiment with Electrolyte I revealed that it achieved a higher level of efficiency due to a 100mV higher open circuit voltage, although the short-circuit current was lower (Table 5.9, Fig. 5.14).

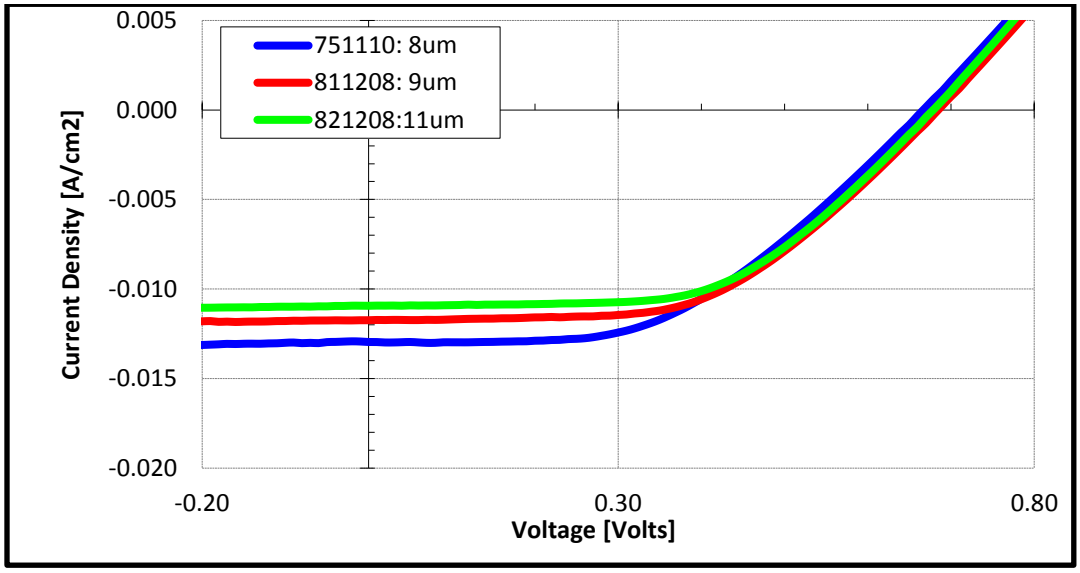

Figure 5.14: Current -voltage relationship for DSC with 'Electrolyte I' at difference thickness. {(Annealing 325/375/450/500ºC - 5ºC/min), (Standard $TiCl_4$ treatment, Anneal 500ºC - 35ºC/min), Black Dye, Electrolyte I, Platisol SP}

Compared to Iodolyte, for 'Electrolyte I' the highest efficiency was also found at a higher thickness, presumably due to the lower viscosity, which would allow it to penetrate deep into the titania layer (Fig. 5.15). This deep penetration should also be the reason of lower J_{sc}, as it would increase the probability of electron recombination with the electrolyte.

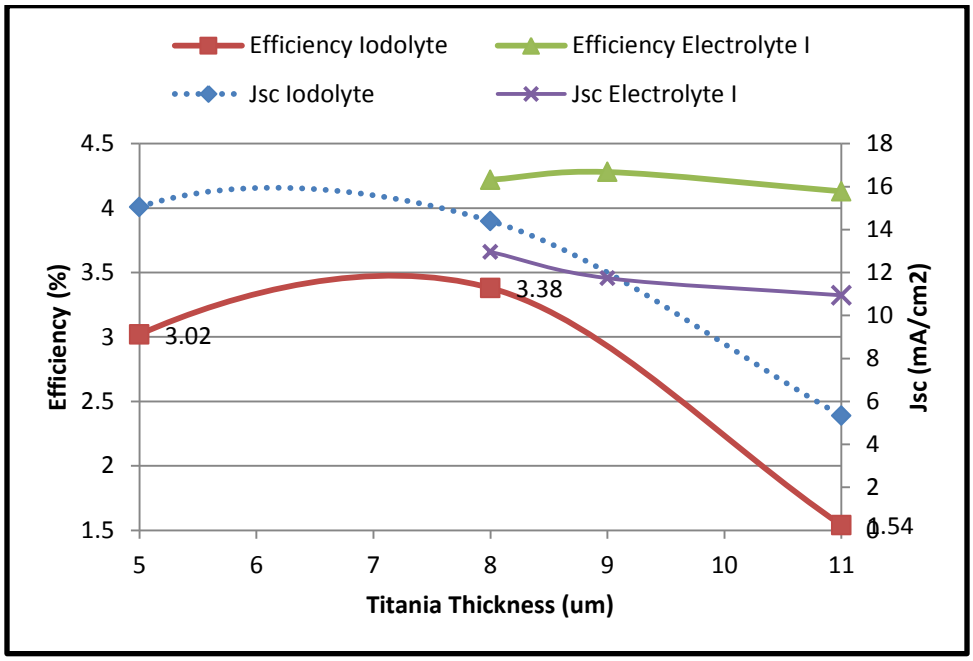

Figure 5.15: Comparison between Iodolyte and Electrolyte I.

Table 5.9: DSC with 'Electrolyte I' at difference thickness

Titania Thickness (um)	V_{oc} (V)	FF	J_{sc} (mA/cm2)	η (%)
8	0.67	0.486	12.96	4.22
9	0.68	0.536	11.74	4.28
11	0.68	0.555	10.94	4.13

5.7 Light Absorption

It was observed that putting a reflective mirror beneath a cell increased its efficiency by increasing current. The fabricated solar cells also looked somewhat transparent. On a typical 11um thick DSC placing a reflective mirror beneath the cell during current voltage measurement showed a current increase of 9%, increasing the efficiency from 4.2% to 4.4% (Fig. 5.16).

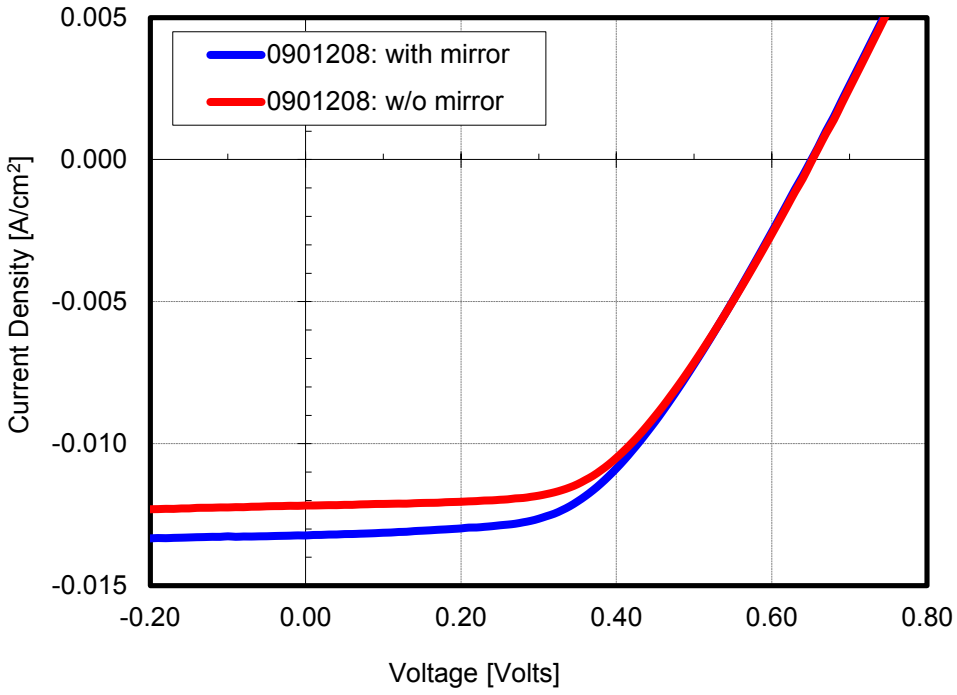

Figure 5.16: Adding a mirror beneath the cell increased its current. {Titania thickness 11um, (Annealing 325/375/450/500ºC - 5ºC/min), (Standard $TiCl_4$ treatment, Anneal 500ºC - 5ºC/min), Black Dye, Electrolyte I}

Although the thickness was optimized for efficiency, the titania film was not absorbing the light efficiently. The reflective mirror was able to return the unabsorbed portion of the light back to the cell, increasing photocurrent. This small experiment suggested that light absorption capability of the titania film was needed to be tuned, keeping the film thickness same. An approach to do that is by introducing a light scattering layer (Section 3.1.2).

5.8 Platinum Electrode

Two types of platinum precursor were used.

- Platisol T (Liquid) – Brush Painted
- Platisol SP (Paste) – Dr Bladed

Higher current as well as higher efficiency was observed for the paste precursor, as it had more platinum content, thus provided more electron exchange center with the electrolyte. The series resistance was also improved. (Table 5.10, Fig. 5.17)

Table 5.10: DSC with different platinum precursor

Platinum Electrode	V_{oc} (V)	FF	J_{sc} (mA/cm^2)	η (%)	R_s (Ω/cm^2)
Platinum Paste	0.63	0.56	10.12	3.6	19.4
Platinum Solution	0.64	0.56	9.56	3.45	20.4

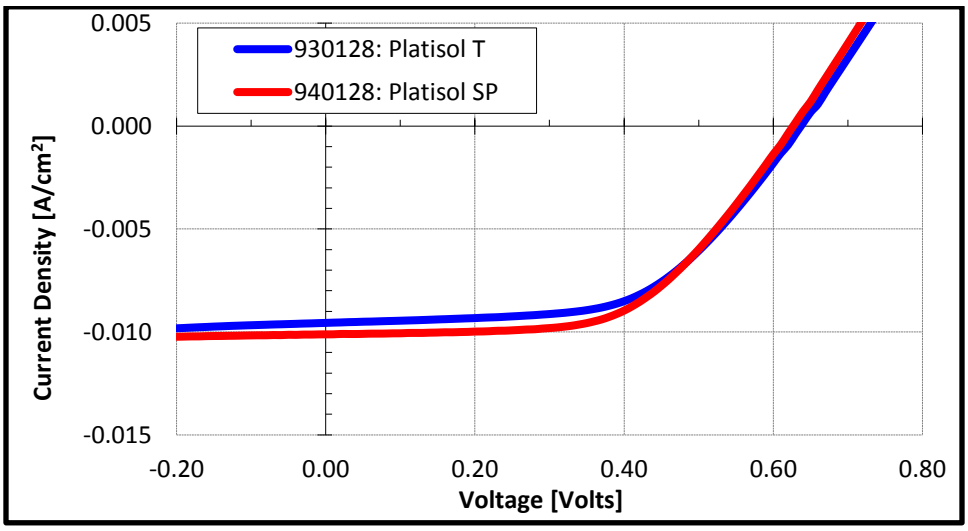

Figure 5.17: Performance comparison between DSC with platinum solution and platinum paste precursor. {Titania thickness 11um, (Annealing 325/375/450/500ºC - 5ºC/min), (Standard $TiCl_4$ treatment, Anneal 500ºC - 35ºC/min), Black Dye, Electrolyte I}

The problem encountered with this paste was that the resultant Pt film was extremely non-uniform & discontinuous (Fig. 5.18), which gave sheet resistances on the order of hundreds of Ωs/sq, when applied on bare glass even when a thick layer of paste was used. In the following experiment, a thick layer of Pt layer was applied by applying more layers of Pt precursor and subsequent annealing. Thus, increasing the thickness of Pt layer reduced the current, presumably due to the increase of series resistance. (Table 5.11, Fig. 5.19)

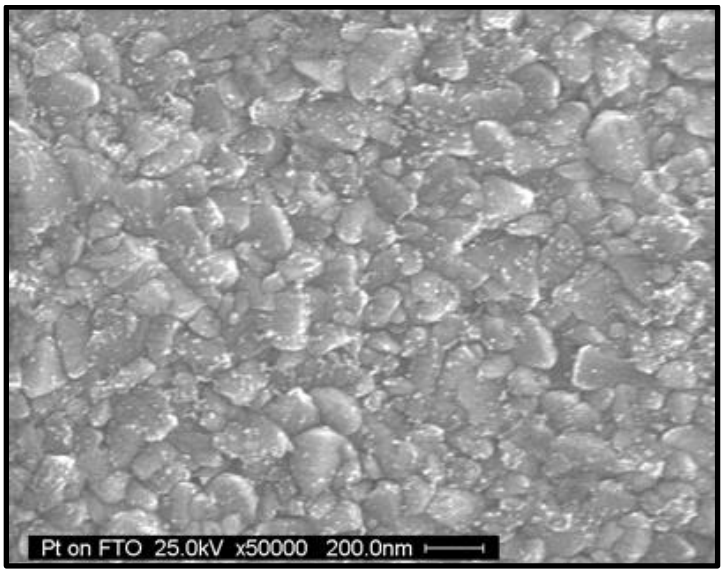

Figure 5.18: SEM image of Pt deposited on FTO coated glass.

Table 5.11: DSC with increased platinum thickness.

Platinum Layer thickness	V_{oc} (V)	FF	J_{sc} (mA/cm^2)	η (%)
3x	0.6	0.542	11.34	3.67
5x	0.6	0.549	10.95	3.58

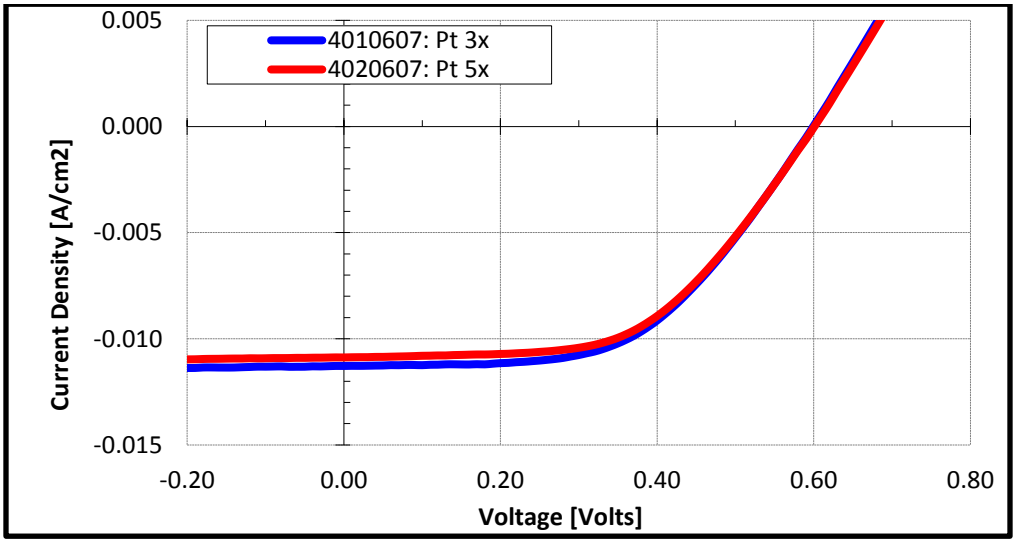

Figure 5.19: Current –voltage relationship for DSC with different platinum thickness. {Titania thickness 9um, (Annealing 325/375/450ºC – 30/10/15ºC/min), (Standard $TiCl_4$ treatment, Anneal 450ºC - 5ºC/min), Black Dye, Electrolyte I, Platisol SP}

Chapter 6: Conclusion and Future Recommendations

This study explored several key parameters towards the optimization of DSC. The conclusion is going to report some future recommendations for further research based on the findings of this study.

As the Titania paste was applied by Dr Blading method, the resulting thickness was a delicate function of the applied pressure, which was controlled manually. To obtain better reproducibility, a screen printing technique may be introduced. The optimum film porosity and surface area was not achieved. It is almost apparent that all different temperature effects were investigated, and the underlying reason was probably chemical components of the titania colloid. Either material from different vendor with different specifications could be examined, or titania paste could be prepared at the laboratory. For optimization of the titania structure, a measurement strategy for surface roughness, effective surface area and film porosity is needed to be introduced. SEM data only gave a raw insight to these parameters.

A light absorbing layer of 400nm diffuse TiO_2 particle is needed. The need for a light absorbing layer is corroborated by the fact that – by placing a mirror beneath the cell, the short circuit current was found to increase. A sputtered platinum electrode may be introduced, to improve charge collection as well as light absorption by reflecting the unabsorbed light back with a mirror action. Some less important enhancements like - soldered contact, anti-reflective coating and low sheet resistance substrates may also be introduced.

References

[1] M. Grätzel, *Solar Energy Conversion by Dye-Sensitized Photovoltaic Cells*, Inorg. Chem., 2005, 44(20), 6841–6851.

[2] First Solar, Inc. (2012), *First Solar, Inc. Announces fourth quarter and 2011 financial results* (Press Release), Retrieved February 28, 2012 from http://investor.firstsolar.com/releasedetail.cfm?ReleaseID=652462

[3] W. Shockley and H. J. Queisser, *Detailed Balance Limit of Efficiency of p-n Junction Solar Cells*, J. Appl. Phys., 1961, 32, 510.

[4] National Renewable Energy Laboratory (2012), Research Cell Efficiency Records, Retrieved September 01, 2012 from http://www.nrel.gov/ncpv/images/efficiency_chart.jpg

[5] T. Marinado, K. Nonomura, J. Nissfolk, M. K. Karlsson, D. P. Hagberg, L. Sun, S. Mori, and A. Hagfeldt, *How the Nature of Triphenylamine-Polyene Dyes in Dye-Sensitized Solar Cells Affects the Open-Circuit Voltage and Electron Lifetimes*, Langmuir, 2010, 26, 2592

[6] National Renewable Energy Laboratory (2012), Reference Solar Spectral Irradiance: Air Mass 1.5, Retrieved September 01, 2012 from http://rredc.nrel.gov/solar/spectra/am1.5/

[7] M. Grätzel, *Recent Advances in Sensitized Mesoscopic Solar Cells*, Acc. Chem. Res., 2009, 42 (11), 1788-1798.

[8] H. Tributsch, *Reaction of Excited Chlorophyll Molecules at Electrodes and in Photosynthesis*; Photochem. Photobiol., 1972, 16, 261-269.

[9] N. Vlachopoulos, P. Liska, J. Augustynski,and M. Graetzel, *Very efficient visible light energy harvesting and conversion by spectral sensitization of high surface area polycrystalline titanium dioxide films*, J. Am. Chem. Soc., 1988, 110 (4), 1216–1220.

[10] B. O'Reagan and M. Grätzel, A Low-Cost, *High-Efficiency Solar Cell Based on Dye Sensitized Colloidal TiO_2 Films,* Nature, 1991, 353, 737-740.

[11] C. Chen, M. Wang, J. Li, N. Pootrakulchote, L. Alibabaei, C. Ngoc-le, J. Decoppet, J. Tsai, C. Grätzel, C. Wu, S. M. Zakeeruddin and M. Grätzel, *Highly Efficient Light-Harvesting Ruthenium Sensitizer for Thin-Film Dye-Sensitized Solar Cells,* ACS Nano, 2009, 3, 3103.

[12] Y. Chiba, A. Islam, Y. Watanabe, R. Komiya, N. Koide and L. Han, *Dye-Sensitized Solar Cells with Conversion Efficiency of 11.1%*, Jpn. J. Appl. Phys., 2006, 45, L638.

[13] A. Yella, H. Lee, H. Tsao, C. Yi, A. Chandiran, M. K. Nazeeruddin, E. Diau, C. Yeh, S. Zakeeruddin, M. Grätzel, *Porphyrin-Sensitized Solar Cells with Cobalt (II/III)-Based Redox Electrolyte Exceed 12 Percent Efficiency*, Science, 2011, 334, 629.

[14] M. Grätzel, *The Advent of Mesoscopic Injection Solar Cells*, Progress in Photovoltaics: Research and Applications, 2006, 14(5), 429-442.

[15] J. Barber and B. Andersson, *Revealing the blueprint of photosynthesis*, Nature, 1994, 370(6484), 31-34.

[16] G. Rothenberger, D. Fitzmaurice and M. Grätzel, *Spectroscopy of conduction band electrons in transparent metal oxide semiconductor films: optical determination of the flatband potential of colloidal titanium dioxide films*, J. Phys. Chem, 1992, 96, 5983-5986.

[17] C. J. Barbé, F. Arendse, P. Comte, M. Jirousek, F. Lenzmann, V. Shklover and M. Grätzel, *Nanocrystalline Titanium Oxide Electrodes for Photovoltaic Applications*, Journal of the American Ceramic Society, 1997, 80(12), 3157–3171.

[18] Q. Wang, S. Ito, M. Grätzel, F. Fabregat-Santiago, I. Mora-Seró, J. Bisquert, T. Bessho, and H. Imai, *Characteristics of High Efficiency Dye-Sensitized Solar Cells*, J. Phys. Chem. B, 2006, 110(50), 25210–25221.

[19] M. Zukalová, A. Zukal, L. Kavan, M. K. Nazeeruddin, P. Liska, and M. Grätzel, *Organized Mesoporous TiO_2 Films Exhibiting Greatly Enhanced Performance in Dye-Sensitized Solar Cells*, Nano Lett., 2005, 5(9), 1789–1792.

[20] T. Kang, A. P. Smith, B. E. Taylor, and M. F. Durstock, *Fabrication of Highly-Ordered TiO_2 Nanotube Arrays and Their Use in Dye-Sensitized Solar Cells*, Nano Lett., 2009, 9(2), 601–606.

[21] A. Hagfeldt, and M. Gratzel, *Light-Induced redox reactions in nanocrystalline systems*, Chem. Rev.,1995, 95, 49–68.

[22] H. Rensmo, K. Keis, H. Lindström, S. Södergren, A. Solbrand, A. Hagfeldt, and S.E. Lindquist, *High Light-to-Energy Conversion Efficiencies for Solar Cells Based on Nanostructured ZnO Electrodes*, J. Phys. Chem. B*,* 1997, 101(14), 2598–2601.

[23] A. Martinson, J. Elam, J. Hupp, and M. Pellin, *ZnO Nanotube Based Dye-Sensitized Solar Cells*; Nano Lett*.,* 2007, 7(8), 2183–2187.

[24] H. J. Snaith, and C. Ducati, *SnO_2-Based Dye-Sensitized Hybrid Solar Cells Exhibiting Near Unity Absorbed Photon-to-Electron Conversion Efficiency*, Nano Lett*.,* 2010, 10(4), 1259–1265.

[25] R. Sharma, R. S. Mane, S. Min, and S. Han, *Optimization of growth of In_2O_3 nano-spheres thin films by electrodeposition for dye-sensitized solar cells,* Journal of Alloys and Compounds, 2009, 479(1-2), 840-843.

[26] A. Kay, and M. Grätzel, *Dye-Sensitized Core−Shell Nanocrystals: Improved Efficiency of Mesoporous Tin Oxide Electrodes Coated with a Thin Layer of an Insulating Oxide*, Chem. Mater., 2002, 14(7), 2930–2935.

[27] A. Le Viet, R. Jose, M. V. Reddy, B. V. R. Chowdari, and S. Ramakrishna, Nb_2O_5 *Photoelectrodes for Dye-Sensitized Solar Cells: Choice of the Polymorph*, J. Phys. Chem. C*,* 2010, 114(49), 21795–21800.

[28] V. Shklover, M. K. Nazeeruddin, S. M. Zakeeruddin, C. Barbé, A. Kay, T. Haibach, W. Steurer, R. Hermann, H. U. Nissen, and M. Grätzel, *Structure of Nanocrystalline TiO_2 Powders and Precursor to Their Highly Efficient Photosensitizer*, Chem. Mater., 1997, 9(2), 430–439.

[29] S. Nakade, M. Matsuda, S. Kambe, Y. Saito, T. Kitamura, T. Sakata, Y. Wada, H. Mori, and S. Yanagida, *Dependence of TiO_2 Nanoparticle Preparation Methods and Annealing Temperature on the Efficiency of Dye-Sensitized Solar Cells*, J. Phys. Chem. B, 2002, 106 (39), 10004-10010.

[30] S. Nakade, Y. Saito, W. Kubo, T. Kitamura, Y. Wada, and S. Yanagida , *Influence of TiO_2 Nanoparticle Size on Electron Diffusion and Recombination in Dye-Sensitized TiO2 Solar Cells*, J. Phys. Chem. B 2003, 107, 8607-8611.

[31] M. K. Nazeeruddin, P. Péchy, T. Renouard, S. M. Zakeeruddin, R. Humphry-Baker, P. Comte, P. Liska, L. Cevey, E. Costa, V. Shklover, L. Spiccia, G. B. Deacon, C. A. Bignozzi, and M. Grätzel, *Engineering of Efficient Panchromatic Sensitizers for Nanocrystalline TiO_2-Based Solar Cells*, J. Am. Chem. Soc., 2001, 123(8), 1613-1624.

[32] M. Grätzel, *Conversion of sunlight to electric power by nanocrystalline dye-sensitized solar cells*, Journal of Photochemistry and Photobiology A: Chemistry, 2004, 164(1–3), 3-14.

[33] S. Ito, M. K. Nazeeruddin, S. M. Zakeeruddin, P. P´echy, P. Comte, M. Gr¨atzel, T. Mizuno, A. Tanaka, and T. Koyanagi, *Study of Dye-Sensitized Solar Cells by Scanning Electron Micrograph Observation and Thickness Optimization of Porous TiO_2 Electrodes*, International J. Photoenergy, 2009, 2009, 517609.

[34] L. Meng, and C. Li, *Blocking Layer Effect on Dye-Sensitized Solar Cells Assembled with TiO_2 Nanorods Prepared by DC Reactive Magnetron Sputtering,* Nanoscience and Nanotechnology Letters, 2011, 3(2), 181–185.

[35] P. J. Cameron and L. M. Peter, *Characterization of Titanium Dioxide Blocking Layers in Dye-Sensitized Nanocrystalline Solar Cells*, J. Phys. Chem. B, 2003, 107, 14394-14400.

[36] A. Burke, S. Ito, H. Snaith, U. Bach, J. Kwiatkowski, and M. Grätzel, *The Function of a TiO_2 Compact Layer in Dye-Sensitized Solar Cells Incorporating "Planar" Organic Dyes*, Nano Lett., 2008, 8(4), 977–981.

[37] S. Ito, T. N. Murakami, P. Comte, P. Liska, C. Grätzel, M. K. Nazeeruddin, M. Grätzel, *Fabrication of thin film dye sensitized solar cells with solar to electric power conversion efficiency over 10%*, Thin Solid Films, 2008, 516(14), 4613–4619.

[38] H. Choi, C. Nahm, J. Kim, J. Moon, S. Nam, D. Jung, and B. Park, *The effect of $TiCl_4$-treated TiO_2 compact layer on the performance of dye-sensitized solar cell,* Current Applied Physics, 2012, 12(3), 737–741.

[39] S. Ito, P. Liska, P. Comte, R. Charvet, P. Péchy, U. Bac, L. Schmidt-Mende, S. M. Zakeeruddin, A. Kay, M. K. Nazeeruddin, and M. Grätzel, *Control of dark current in photoelectrochemical (TiO_2/I^-- I_3^-) and dye-sensitized solar cells,* Chem. Commun., 2005, 34, 4351-4353.

[40] E. Palomares, J. N. Clifford, S. A. Haque, T. Lutz, and J. R. Durrant, *Control of Charge Recombination Dynamics in Dye Sensitized Solar Cells by the Use of Conformally Deposited Metal Oxide Blocking Layers,* J. Am. Chem. Soc., 2003, 125(2), 475–482.

[41] Z. Wang, T. Yamaguchi, H. Sugihara, and H. Arakawa, Significant Efficiency *Improvement of the Black Dye-Sensitized Solar Cell through Protonation of TiO_2 Films, Langmuir*, 2005, 21(10), 4272–4276.

[42] Y. V. Zubavichus, Y. L. Slovokhotov, M. K. Nazeeruddin, S. M. Zakeeruddin, M. Grätzel, and V. Shklover, *Structural Characterization of Solar Cell Prototypes Based on Nanocrystalline TiO_2 Anatase Sensitized with Ru Complexes. X-ray Diffraction, XPS, and XAFS Spectroscopy Study*, Chem. Mater., 2002, 14(8), 3556–3563.

[43] S. M. Zakeeruddin, M. K. Nazeeruddin, P. Pechy, F. P. Rotzinger, R. Humphry-Baker, K. Kalyanasundaram, M. Grätzel, V. Shklover and T. Haibach, *Molecular Engineering of Photosensitizers for Nanocrystalline Solar Cells: Synthesis and Characterization of Ru Dyes Based on Phosphonated Terpyridines*, Inorg. Chem., 1997, 36 (25), 5937–5946.

[44] M. K. Nazeeruddin, P. Péchy, T. Renouard, S. M. Zakeeruddin, R. Humphry-Baker, P. Comte, P. Liska, L. Cevey, E. Costa, V. Shklover, L. Spiccia, G. B. Deacon, C. A. Bignozzi and M. Grätzel, *Engineering of Efficient Panchromatic Sensitizers for Nanocrystalline TiO_2-Based Solar Cells*, J. Am. Chem. Soc., 2001, 123, 1613.

[45] M. Grätzel, and J. Durrant, *Dye-Sensitised Mesoscopic Solar Cells*. In M. Archer and A. Nozik (Eds.), *Nanostructured And Photoelectrochemical Systems For Solar Photon Conversion* (pp. 503-536), Imperial College Press.

[46] M. K. Nazeeruddin, A. Kay, I. Rodicio, R. Humphry-Baker, E. Mueller, P. Liska, N. Vlachopoulos, M. Graetzel, *Conversion of light to electricity by cis-X2bis(2,2'-bipyridyl-4,4'-dicarboxylate)ruthenium(II) charge-transfer sensitizers (X = Cl-, Br-, I-, CN-, and SCN-) on nanocrystalline titanium dioxide electrodes*, J. Am. Chem. Soc., 1993, 115(14), 6382–6390.

[47] M. K. Nazeeruddin, P. Péchy and M. Grätzel, *Efficient panchromatic sensitization of nanocrystallineTiO_2 films by a black dye based on a trithiocyanato–ruthenium complex*, Chem. Commun., 1997, 18, 1705-1706.

[48] M. K. Nazeeruddin, R. Humphry-Baker, P. Liska, and M. Grätzel, *Investigation of Sensitizer Adsorption and the Influence of Protons on Current and Voltage of a Dye-Sensitized Nanocrystalline TiO_2 Solar Cell*, J. Phys. Chem. B, 2003, 107(34), 8981–8987.

[49] M. K. Nazeeruddin, S. M. Zakeeruddin, R. Humphry-Baker, M. Jirousek, P. Liska, N. Vlachopoulos, V. Shklover, C. H. Fischer, and M. Grätzel, *Acid−Base Equilibria of (2,2'-Bipyridyl-4,4'-dicarboxylic acid)ruthenium(II) Complexes and the Effect of Protonation on Charge-Transfer Sensitization of Nanocrystalline Titania*, Inorg. Chem., 1999, 38(26), 6298–6305.

[50] M. K. Nazeeruddin, R. Humphry-Baker, M. Grätzel, and B. A. Murrer, *Efficient near IR sensitization of nanocrystalline TiO_2 films by ruthenium phthalocyanines*, Chem. Commun., 1998, 6, 719-720.

[51] Q. Wang, W. M. Campbell, E. E. Bonfantani, K. W. Jolley, D. L. Officer, P. J. Walsh, K. Gordon, R. Humphry-Baker, M. K. Nazeeruddin, and M. Grätzel, Efficient Light Harvesting by Using Green Zn-Porphyrin-Sensitized Nanocrystalline TiO_2 Films, J. Phys. Chem. B, 2005, 109(32), 15397–15409.

[52] J. N. Clifford, E. Palomares, M. K. Nazeeruddin, M. Grätzel, J. Nelson, X. Li, N. J. Long, and J. R. Durrant, *Molecular Control of Recombination Dynamics in Dye-Sensitized Nanocrystalline TiO_2 Films: Free Energy vs Distance Dependence*, J. Am. Chem. Soc., 2004, 126(16), 5225–5233.

[53] J. Lagref, M. K. Nazeeruddin, and M. Grätzel, *Molecular engineering on semiconductor surfaces: design, synthesis and application of new efficient amphiphilic ruthenium photosensitizers for nanocrystalline TiO_2 solar cells*, Synthetic Metals, 2003, 138, 333–339.

[54] C. Klein, M. K. Nazeeruddin, D. Censo, P. Liska, and M. Grätzel, *Amphiphilic Ruthenium Sensitizers and Their Applications in Dye-Sensitized Solar Cells*, Inorg. Chem., 2004, 43(14), 4216–4226.

[55] J. N. Clifford, E. Palomares, M. K. Nazeeruddin, R. Thampi, M. Grätzel, and J. R. Durrant, *Multistep Electron Transfer Processes on Dye Co-sensitized Nanocrystalline TiO_2 Films*, J. Am. Chem. Soc., 2004, 126(18), 5670–5671.

[56] M. K. Nazeeruddin, R. Humphry-Baker, D. L. Officer, W. M. Campbell, A. K. Burrell and M. Grätzel, *Application of metalloporphyrins in nanocrystalline dye-sensitized solar cells for conversion of sunlight into electricity,* Langmuir 20(15), 2004, 6514-6517.

[57] Y. Chang, C. Wang, T. Pan, S. Hong, C. Lan, H. Kuo, C. Lo, H. Hsu, C. Lin, and E. Diau, *A strategy to design highly efficient porphyrin sensitizers for dye-sensitized solar cells*, Chem. Commun., 2011, 47, 8910-8912.

[58] W. M. Campbell, K. W. Jolley, P. Wagner, K. Wagner, P. J. Walsh, K. C. Gordon, L. Schmidt-Mende, M. K. Nazeeruddin, Q. Wang, M. Grätzel, and D. L. Officer, *Highly Efficient Porphyrin Sensitizers for Dye-Sensitized Solar Cells*, J. Phys. Chem. C, 2007, 111(32), 11760–11762.

[59] W. M. Campbell, A. K. Burrell, D. L. Officer, K. W. Jolley, *Porphyrins as light harvesters in the dye-sensitised TiO2 solar cell*, Coordination Chemistry Reviews, 2004, 248, 1363–1379.

[60] J. Wu, Z. Lan, S. Hao, P. Li, J. Lin, M. Huang, L. Fang, and Y. Huang, *Progress on the electrolytes for DSSC*, Pure Appl. Chem., 2008, 80(11), 2241-2258.

[61] L. Han, N. Koide, Y. Chiba, A. Islam, R. Komiya, N. Fuke, A. Fukui and R. Yamanaka, *Improvement of efficiency of dye-sensitized solar cells by reduction of internal resistance*, Appl Phys Lett, 2005, 86, 213501–213503.

[62] L. Zeng, S. Dai, K. Wang, X. Pan, C. Shi, L. Guo, *Mechanism of Enhanced Performance of Dye-Sensitized Solar Cell Based TiO_2 Films Treated by Titanium Tetrachloride*, Chinese Physics Letters, 2004, 21(9), 1835-1837.

Appendices

Appendix A: Image Copyright Information

Figure 1.1 : Reprinted from Research Cell Efficiency Records, NREL, http://www.nrel.gov/ncpv/images/efficiency_chart.jpg (Retrieved September 01, 2012), Copyright © 2012, with permission from National Renewable Energy Laboratory.

Figure 2.2 : Reprinted from J. Phys. Chem. B, Volume 110 (50), Pages 25210–25221, Q. Wang, S. Ito, M. Grätzel, F. Fabregat-Santiago, I. Mora-Seró, J. Bisquert, T. Bessho, and H. Imai, *Characteristics of High Efficiency Dye-Sensitized Solar Cells*, Copyright © 2006, with permission from American Chemical Society.

Figure 3.2 : Reprinted from *Dye-Sensitised Mesoscopic Solar Cells,* M. Grätzel, and J. Durrant, in *Nanostructured And Photoelectrochemical Systems For Solar Photon Conversion,* M. Archer and A. Nozik (Eds.), pp. 503-536, Copyright © 2008 Imperial College Press.

Figure 3.3 : Reprinted from Ruthenizer 620-1H3TBA, Solaronix SA, http://www.solaronix.com/products/rutheniumdyes/ruthenizer6201h3tba/ (Retrieved September 07, 2012), Copyright © 2012, with permission from Solaronix SA.

Figure 3.4 : Reprinted from Science, Volume 334, No. 6056, Pages 629-634, A. Yella, H. Lee, H. Tsao, C. Yi, A. Chandiran, M. K. Nazeeruddin, E. Diau, C. Yeh, S. Zakeeruddin, and M. Grätzel, *Porphyrin-Sensitized Solar Cells with Cobalt (II/III)-Based Redox Electrolyte Exceed 12 Percent Efficiency*, Copyright © 2011, with permission from AAAS.

Figure 3.5 : Reprinted from Journal of Photochemistry and Photobiology A: Chemistry, Volume 164, Issues 1–3, Pages 3–14, Michael Grätzel, *Conversion of sunlight to electric power by nanocrystalline dye sensitized solar cells*, Copyright © 2004, with permission from Elsevier.